Developmental effects of oxytocin neurons on social affiliation and processing of social information

Ana Rita Nunes[1,2,*], Michael Gliksberg[2,*], Susana A.M. Varela[1,3], Magda Teles[1], Einav Wircer[2], Janna Blechman[2], Giovanni Petri[4], Gil Levkowitz[2,#], Rui F. Oliveira[1,3,5,#]

* These authors contributed equally to the work

[1] Integrative Behavioural Biology Lab, Instituto Gulbenkian de Ciência, Oeiras 2780-156, Portugal.

[2] Department of Molecular Cell Biology, Weizmann Institute of Science, Rehovot 7610001, Israel.

[3] ISPA- Instituto Universitário, Lisboa 1149-041, Portugal

[4] ISI Foundation & ISI Global Science Foundation, 10126 Torino, Italy

[5] Champalimaud Research, Champalimaud Centre for the Unknown, 1400-038 Lisbon, Portugal.

Correspondence should be addressed to

G.L. gil.levkowitz@weizmann.ac.il

R.F.O. ruiol@ispa.pt

Abbreviated title: Oxytocin effects on development of the social brain

30 pages; 6 main figures; 14 extended data figures.

Abstract- 174 words; Introduction- 505 words; Discussion- 782 words

KEYWORDS: Sociality, oxytocin, dopamine, zebrafish, development, organizational hypothesis, social decision making network

Conflict of interest: The authors declare no competing financial interests

ACKNOWLEDGMENTS

We thank all members of Gil Levkowitz´s and Rui Oliveira´s laboratories for fruitful discussions, and Nitzan Konstantin for English editing. We thank the technical support of IGC's Advanced Imaging Facility (AIF-UIC), which is supported by the national Portuguese funding ref# PPBI-POCI-01-0145-FEDER-022122, co-financed by Lisboa Regional Operational Programme (Lisboa 2020), under the Portugal 2020 Partnership Agreement, through the European Regional Development Fund (FEDER) and Fundação para a Ciência e Tecnologia (FCT, Portugal); all the staff from the Fish Facility platforms of Instituto Gulbenkian de Ciência, Portugal, and Weizmann Institute of Science, Israel, for animal care and valuable advice; Congento, which is supported by the funding ref# LISBOA-01-0145-FEDER-022170, co-financed by Lisboa Regional Operational Programme (Lisboa 2020), under the Portugal 2020 Partnership Agreement, through the European Regional Development Fund (FEDER) and Fundação para a Ciência e a Tecnologia (FCT; Portugal); IGC´s Histopathology Facility for technical support, help and valuable advices; the Advanced BioImaging and BioOptics Experimental Platform (ABBE Platform) of the Champalimaud Center for the Unknown (CCU) for all the technical support and help.

Abstract

Hormones regulate behavior either through activational effects that facilitate the acute expression of specific behaviors or through organizational effects that shape the development of the nervous system thereby altering adult behavior. Much research has implicated the neuropeptide oxytocin (OXT) in acute modulation of various aspects of social behaviors across vertebrate species, and OXT signaling is associated with the developmental social deficits observed in autism spectrum disorders, however, little is known about the role of OXT in the neurodevelopment of the social brain. We show that perturbation of OXT neurons during early zebrafish development led to a loss of dopaminergic neurons, associated with visual processing and reward, and blunted the neuronal response to social stimuli in the adult brain. Ultimately, adult fish whose OXT neurons were ablated in early life, displayed altered functional connectivity within social decision-making brain nuclei both in naïve state and in response to social stimulus and became less social. We propose that OXT neurons have an organizational role, namely to shape forebrain neuroarchitecture during development and to acquire an affiliative response towards conspecifics.

Significance Statement:

Social behavior is developed over the lifetime of an organism and the neuropeptide oxytocin modulates social behaviors across vertebrate species, and is associated with neuro-developmental social deficits such as autism. However, whether oxytocin plays a role in the developmental maturation of neural systems that are necessary for social behavior remains poorly explored. We show that proper behavioral and neural response to social stimuli depends on a developmental process orchestrated by oxytocin neurons. Animals whose oxytocin system is ablated in early life show blunted neuronal and behavioral responses to social stimuli as well as wide ranging disruptions in the functional connectivity of the Social Brain. We provide a window into the mechanisms underlying oxytocin-dependent developmental processes that implement adult sociality.

INTRODUCTION

Social behavior describes any of a wide group of behaviors by an organism towards members of its species, termed conspecifics (Robinson et al., 2019). The systems underlying these behaviors are thought to be established during development whereas the behavioral manifestations themselves are not immediately put into effect, but become apparent only later in life.

The “organizational hypothesis” claims that hormones can shape the structure of the developing nervous system and as a result alter the adult animal behavior and was first suggested by Phoenix, et al. following their study of the developmental effect of testosterone exposure on subsequent sexual behavior (Phoenix et al., 1959). Organizational effects refer to long-term, irreversible impact of hormones on tissue differentiation that can either directly or indirectly influence physiology, metabolism and behavior. In the context of behavior, organizational signals that can be mediated by neuropeptides, are necessary during critical developmental windows in order to shape neural systems whose activity will only become relevant at a later stage in the lifetime of the animal. This organizational effect is contrasted with the acute or “activational” effect exerted by hormones, neurotransmitters and neuropeptides on behavior, physiology and metabolism.

The neuropeptide oxytocin (OXT) has a widely-studied activational role in several aspects of social behavior (for a review see (Donaldson and Young, 2008; Grinevich et al., 2016; Jurek and Neumann, 2018)), including social processing (Gamer et al., 2010; Grinevich and Stoop, 2018), attention (Bartz et al., 2011; Lukas et al., 2011; Shamay-Tsoory and Abu-Akel, 2016), reward (Insel and Shapiro, 1992; Bowen and Neumann, 2017), and pro-social behaviors (Lukas et al., 2011), in rodents and humans. Previously, we showed that this activational role of OXT is evolutionarily conserved in deep time, since OXT also modulates perception of visual social cues (Nunes et al., 2020) and social recognition (Ribeiro et al., 2020a, 2020b) in zebrafish.

OXT is thought to have organizational effects as well. As early as 1989, Noonan et al. showed that pharmacological treatment of neonatal rats with OXT had long term effects

on behavior in the adult (Noonan et al., 1989). In a more recent example, Keebaugh and Young utilized selective viral overexpression to modulate OXTR levels in the nucleus accumbens of pre-pubertal female prairie voles and showed that this developmental intervention is necessary and sufficient to induce alloparental behavior in the adult (Keebaugh and Young, 2011). Such results have been described in various mammalian models, behavioral domains, and using pharmacological (e.g. peptide, agonist and antagonist injection) as well as genetic interventions in prenatal and prepubertal animals (for a review see (Miller and Caldwell, 2015) and (Hammock, 2015)). Furthermore, human studies of Autism Spectrum Disorder (ASD) have strongly suggested that certain features of ASD arise from very early developmental abnormalities which are thought to be linked to OXT signaling, further suggesting an organizational role for OXT in the development of social behavior (Heinrichs et al., 2009; Hovey et al., 2014) or for a review (Guastella and Hickie, 2016). However, the mechanisms underlying this organizational mode of action have thus far remained elusive.

It has been well established that oxytocin communicates with other neurotransmitter systems for proper social behaviors. Dopamine (DA) is mainly involved in reward and reinforcement systems (Dölen and Malenka, 2014; Love, 2014), but also in sensory modulation and attention gating (Love, 2014; Grinevich et al., 2015). DA neurons are activated during social interactions and mating, and interact with the OXT system to promote pair-bond formation (Dölen and Malenka, 2014; Johnson et al., 2017) and sociability (Hung et al., 2017), suggesting that OXT and dopamine are both necessary to promote the sensory and rewarding aspects of social interactions.

Here, we show that in zebrafish, signaling by OXT neurons is required in an organizational manner during early life for the display of social affiliation in adulthood. Furthermore, we go on to show that perturbing this process in a very early developmental time window, equivalent to fetal developmental stages in mammals, has long-lasting effects on specific dopaminergic clusters associated with reward and visual attention/ processing, and also leads to wide-ranging changes in brain activity within previously described social processing networks.

MATERIALS AND METHODS

Experimental model

Zebrafish were raised and bred according to standard protocols. Zebrafish were kept in mixed sex groups (10 adults/l) in a recirculation life supporting system (tecniplast) with the following parameters: 28 °C, pH 7.0, conductivity 1000 µS/cm, 14 L:10D light:dark cycle. Fishes were fed with a combination of live food (Paramecium caudatum and Artemia salina) and commercial processed dry food (Gemma). Husbandry protocols, water chemistry and health program have been described previously (Borges et al., 2016). All experimental procedures were conducted in accordance with standard operating procedures of the Instituto Gulbenkian de Ciência and Direcção Geral de Alimentação e Veterinária (DGAV- Direcção Geral de Alimentação e Veterinária, permit number 0421/000/000/2015), Portugal, and Institutional Animal Care and Use Committee (IACUC, protocol number 27100516) of the Weizmann Institute, Israel.

Zebrafish transgenic/mutant lines used in this study: *Tg(oxt:EGFP*)(Blechman et al., 2011), *Tg(oxt:Gal4)wz06* (Anbalagan et al., 2018), *Tg(UAS:NTR-mCherry)c264* (Davison et al., 2007), *Tg(UAS:sypb-EGFP)* (Meyer and Smith, 2006).

Larvae and adult zebrafish (3-6 months old) of both sexes were used in this work.

Social affiliation assay

The social preference test followed the protocol described previously (Wircer et al., 2017; Ribeiro et al., 2020a). Briefly, focal zebrafish were given a choice between two side-by-side compartments: one containing a shoal (two males and two females) and an empty one (Figure 1A-B) during a 10-min test. The stimulus shoal matched the genotype of the focal fish. The stimulus compartment was randomly switched between tests, to control for any place preference possibly induced by the arena or laboratory frames. All compartments were completely sealed to block transmission of chemical and vibrational stimuli and thus, only visual cues were accessible. The experimental test tank was placed over a custom-built infrared LED light box, to increase image quality for subsequent

115 automated video tracking. Fish behavior was recorded from above with either a high-
116 speed camera FLARE (2M360, Io Industries) or a B&W mini surveillance camera
117 (Henelec 300B) connected to a computer, using video recording software (Pinnacle
118 Studio 12). Videos were analyzed with Ethovision XT11.0 (Noldus Inc., The Netherlands).
119 Relevant data were then exported and further analyzed. The two regions of interest,
120 empty and shoal, were defined as the 1/10 of the length of the arena immediately adjacent
121 to the empty compartment or the compartment containing the stimulus shoal,
122 respectively. The percentage of cumulative time fish spent in these regions of interest
123 ($\%T_{shoal}$ and $\%T_{empty}$) was used to calculate the social affiliation score [$\%T_{shoal}/(\%T_{shoal}$
124 $+\%T_{empty})$]. This score, also called the sociability score, has been commonly used in
125 rodent studies to measure sociability in the 3-chamber test (Park et al., 2018). Total
126 distance traveled was also measured.

127 **Ontogeny of social affiliation behavior**: Social preference was tested at different
128 developmental stages: early larvae (12 days-old), mid larvae (14-20 days-old), post-
129 flexion metalarvae (21-30 days-old), juveniles and adults (from 30 to 90 days-old). The
130 size of the testing arena for early larvae was 3.5 x 6.0 cm; for mid larvae 7.0 x 8.0 cm; for
131 metalarvae 7.0 x 10.0 cm; and for juveniles and adults it was 20.0 X 20.0 cm. The stimulus
132 shoal matched the developmental stage of the focal fish. Two different experiments were
133 performed: a) longitudinal, where individual fish were repeatedly tested at each
134 developmental time point, and b) cross-sectional, where individual fish were tested only
135 once, at a given developmental time point.

136 From all behavioral experiments, animals were excluded from analysis if they failed to
137 enter both the ROIs (i.e. Shoal and Empty) as this results in a social score equals to
138 infinity.

139

140 **Chemically induced OXT neuronal ablation**

141 **Early ablation**: Nitroreductase (NTR)-mediated cellular chemically induced OXT
142 neuronal ablation was conducted as previously described(Curado et al., 2007, 2008).
143 Briefly, larvae (~30-40 per petri dish) were treated with metronidazole (MTZ, Vetranal
144 CAT#46461, Sigma) dissolved in Danieau buffer to a final concentration of 10mM for 48

145 h while being protected from light, to prevent MTZ photoinactivation. After the first 24 h,
146 the MTZ-containing Danieau buffer was replaced by fresh MTZ medium. Control
147 untreated larvae were subjected to the same procedure in Danieau buffer without MTZ,
148 but were also protected from light. After 48 h of treatment, larvae were washed out several
149 times in Danieau buffer.

150 **Adult ablation**: We used a modified ablation protocol of 3X48 h MTZ treatments (5 mM),
151 as we observed that this increased survival of adult animals. Briefly, adult zebrafish were
152 placed into 2-liter tanks containing MTZ (Veterinary preparation, Vetmarket; Shoham,
153 Israel, CAT#165228, or 2-methyl-5-nitroimidazole-1-ethanol, TCL Europe, CAT#M0924)
154 dissolved in system water at a final concentration of 5 mM, protected from light. After ~16
155 h of treatment, zebrafish were moved to a tank containing fresh system water without
156 MTZ, fed, and allowed to recover for ~2 h, followed by a second treatment of MTZ 5mM
157 for 16 h. Animals were then allowed to recover in their home tanks for 48 h. The entire
158 protocol was repeated three times.

159 **Effect of chemically induced OXT neuronal ablation on endogenous OXT cells.**
160 Zebrafish treated with MTZ at different time points during development (4-6 days-old, 12-
161 14 days-old, 20-22 days-old or 90 days-old) were allowed to recover from treatment for
162 48 h and were then sacrificed to assess the treatment effects on endogenous OXT cells
163 by *in situ* hybridization (see below) or by direct visualization of the mCherry transgene
164 signal. OXT cells were manually counted using imageJ software (Schindelin et al., 2012),
165 except for *in situ* experiment at 22-24 days-old where we used a semi-automated method
166 for quantifying total fluorescence (see below).

167 **Recovery of endogenous OXT cells following early-life chemically induced OXT**
168 **neuronal ablation.** Zebrafish larvae were ablated at 12-14 DPF, and then allowed to
169 grow until adulthood. At 90 DPF animals were sacrificed, brains harvested, and subjected
170 to fluorescent in situ hybridization (see below). The total fluorescence was then quantified
171 in a semi-automated manner (see below).

172 **Effect of chemically induced OXT neuronal ablation on adult social affiliation.**
173 Zebrafish treated with MTZ at 4-6 days-old, 12-14 days-old, 20-22 days-old or 90 days-

174 old were allowed to grow until adulthood to be tested for social affiliation behavior (see
175 above).

176 **Time course of NTR-mCherry recovery following 4-6 days-old chemically induced**
177 **OXT neural ablation.** Fish were treated with MTZ at 4-6 days-old and sampled at
178 different time points: 8, 12, 19, 26 and 42 days-old.

179 **Semi-automated method for quantifying total fluorescence.** For quantification of
180 images in the recovery experiment, and the effect of ablation at 22-24 DPF on OXT mRNA
181 we utilized a semi-automated method for quantifying total fluorescence. Each Z-stack was
182 broken into its component optical planes, and ROI's were selected for the region
183 containing the cells and the background (a region within the tissue with no fluorescent
184 cells). The threshold for "positive" pixels was defined as the 75th percentile value of al
185 the pixels in the background ROI, and all positive pixels per slice were counted. the total
186 number of positive pixels per sample was summed, and then normalized to the maximal
187 value for that cohort. Source code in MATLAB for this procedure is included.

188 **Effect of 4-6 days-old chemically induced OXT neuronal ablation on adult neuronal**
189 **activity (pS6 activation).** To assess the effect of early OXT ablation on adult brain
190 activation patterns in response to a social stimulus, adult zebrafish that had been treated
191 with MTZ at 4-6 days-old and untreated controls were exposed individually to either a
192 mixed-sex shoal of conspecifics or an empty tank for 10 min. Immediately after, we
193 blocked the visual stimulus, without disturbing the focal fish, by placing an opaque
194 partition between the experimental and stimulus tanks. After 50 min (to allow for
195 expression of the pS6 neural activation marker), zebrafish were sacrificed and heads
196 were collected and processed for paraffin slice immunofluorescence (see below).

197 **Effect of 4-6 days-old chemically induced OXT neuronal ablation on larvae and**
198 **adult dopaminergic system.** Untreated and 4-6 days-old MTZ-treated zebrafish larvae
199 were allowed to recover from treatment (48h) and were either processed immediately for
200 whole-mount larvae TH immunofluorescence (see below) or allowed to grow until
201 adulthood and then processed for paraffin slice TH-immunofluorescence (see below).

202

203 **In situ hybridization**

204 RNA *in situ* hybridization was performed on both whole larvae and whole adult brains.
205 Larvae or dissected brains were fixed in 4%PFA and *in situ* hybridization was performed
206 as described in (Machluf and Levkowitz, 2011; Wircer et al., 2017). An OXT probe was
207 generated using a pGEM plasmid encoding for *oxt* mRNA (RefSeq NM_178291.2).
208 Following development with Fast Red reagent (Roche, cat. No. 11496549001), adult
209 brains were embedded in agar and sagittally cut at a thickness of 150µm on a vibratome,
210 and whole larvae and brain slices were mounted in glycerol and imaged on a Zeiss LSM
211 800 scanning confocal microscope.

212

213 **Whole-mount larvae immunofluorescence**

214 Briefly, larvae were euthanized in ice-cold water, transferred to 4% PFA and then
215 incubated overnight at 4°C on a shaker. Then, the PFA was washed out and samples
216 were placed in pre-cooled acetone in a freezer at -20°C for 10 min. The acetone was
217 washed out (PBS 0.1% TritonX-100), and the samples were then incubated in blocking
218 solution (PBS 0.1% triton + 1% DMSO + 1% BSA + 5% NGS) for minimum of 2 h at room
219 temperature (RT), followed by incubation with primary antibody overnight at 4ºC on a
220 shaker. Primary antibodies used were either mouse anti-TH (MAB 318, Merck Millipore),
221 rabbit anti-EGFP (A11122, ThermoFisher) or guinea pig anti-OXT (T-5021, Peninsula
222 labs), at a concentration of 1:200. Next, samples were washed repeatedly (minimum of
223 6X15 min washes) with blocking solution and then placed in a blocking solution containing
224 fluorescent secondary antibody (1:200) overnight at 4ºC on a shaker. Then, samples were
225 washed in PBS, mounted dorsally on a slide in mounting medium (Aqua-Polymount,
226 Polysciences Inc., Warrington PA, CAT# 18606-20) and imaged by a Zeiss LSM 800
227 scanning confocal microscope.

228

229 **Paraffin adult brain slice immunofluorescence**

230 Zebrafish heads were fixed in 10% buffered formalin for 72 h and decalcified in EDTA
231 (0.5 M, pH 8.0) for 48 h, followed by paraffin inclusion. Coronal slices (6 µm-thick) were

232 cut with a microtome. Sectioned slices were then processed for immunofluorescence.
233 After antigen retrieval with Tris-EDTA (10 mM Tris Base, 1 mM EDTA, 0.05% Tween20)
234 at 95ºC for 20 min, slices were washed in TBS-Tx (TBS 0.025% TritonX-100, 3X10 min),
235 then incubated with blocking solution (TBS 0.025% TritonX-100 + 1%BSA) for 1 h at RT,
236 followed by an overnight incubation with a primary antibody (1:400 at 4ºC). Slides were
237 then washed in TBS- 0.025% TritonX-100 (3X10 min) and incubated in secondary
238 antibody (1:1000 for 2 h). After washes, slices were incubated with DAPI for 20 min, then
239 rinsed in TBS and mounted with EverBrite™ Hardset Mounting medium (Biotium).
240 Primary antibodies used were anti-phosphorylation of S6 ribosomal protein, pS6 (Cell
241 signaling S235/236) and anti-tyrosine hydroxylase, anti-TH, (mouse monoclonal, MAB
242 318, Merck Millipore).

243 **Neuronal quantifications**

244 **Neuronal pS6 cell quantification**

245 Coronal images were acquired with a commercial Nikon High Content Screening
246 microscope, based on Nilon Ti equipped with a Andor Zyla 4.2 sCMOS camera, using a
247 20X 0.75 NA objective, quadruple dichroic filter, and controlled with the Nikon Elements
248 software. To avoid double-imaging of the same cells, we imaged every other slice. We
249 quantified density of pS6-positive cells in 16 brain areas that belong to the social decision
250 making network (O'Connell and Hofmann, 2011): Vv- ventral nucleus of the ventral
251 telencephalic area (V), homologous to the mammalian lateral septum, subdivided into:
252 anterior (Vv_a) and posterior (Vv_p); Vd- dorsal nucleus of V, homologous to the
253 mammalian Nacc, subdivided into: anterior (Vd_a), medial (Vd_m) and posterior (Vd_p);
254 Vc- central nucleus of V, homologous to the mammalian striatum, subdivided into: anterior
255 (Vc_a) and posterior (Vc_p); Dm- medial zone of the dorsal telencephalic area (D),
256 homologous to the mammalian bLAMY; Dl- lateral zone of D, homologous to
257 hippocampus; Dd- dorsal zone of D; Vs- supracommissural nucleus of V, homologous to
258 the mammalian extended amygdala (BNST and meAMY); Vp- postcommissural nucleus
259 of V; Ppa- parvocellular preoptic nucleus, anterior part and Ppp- parvocellular preoptic
260 nucleus, posterior part, both homologous to the mammalian preoptic area; VM-
261 ventromedial thalamic nucleus; VL-ventrolateral thalamic nucleus (Figure 6-1).

262 For each brain area, about five coronal brain slices were analyzed manually using imageJ
263 software (Schindelin et al., 2012). Background subtraction and linear adjustments of
264 brightness and contrast levels were performed in the same way for all groups. The brain
265 areas of interest were identified using DAPI to define neuroanatomical boundaries and
266 landmarks identified in the Zebrafish Atlas (Wullimann and Mueller, 2004). In each brain
267 slice, we placed one square of 1000 μm^2 in the brain region of interest, in each
268 hemisphere, following these criteria: the square was always placed over the highest
269 number of pS6-positive cells, keeping minimum distance from the border and edge of the
270 brain section, a similar strategy that has been used by others (Lorenzi et al., 2017). pS6-
271 positive cells were counted if a nucleus surrounded by the cytoplasm was clearly visible,
272 and if the intensity of the pS6 signal was perceptibly greater than background (see Figure
273 6 for examples of pS6 staining in the sampled brain areas).

274

275 **Dopaminergic neuronal quantification**

276 Dopaminergic quantification was performed in both larvae and adult zebrafish, either 4-6
277 days-old MTZ-treated or untreated. Briefly, for larvae, whole-mount zebrafish
278 immunofluorescence was performed as described above using primary antibody anti-TH.
279 Larvae were imaged and confocal z-stacks were analyzed by ImageJ. Larva
280 dopaminergic forebrain, pretectum and posterior tuberculum nucleus were identified
281 according to (Sallinen et al., 2009; Tay et al., 2011) and TH+ cells were counted in these
282 three groups.

283 For adults, heads from both treatment groups (untreated and 4-6 days-old MTZ-treated)
284 were collected and processed for paraffin embedding, followed by paraffin slice
285 immunofluorescence as described above. Coronal slices were acquired with a
286 SlideScanner Zeiss AxioScan Z1 (Zeiss), and analyzed with Zeiss Zen Lite software. To
287 avoid double-imaging of the same cells, we imaged every other slice. Boundaries
288 separating brain nuclei and subdivisions were identified based on DAPI staining, using as
289 reference a coronal atlas of the zebrafish (Wullimann et al., 1996). Dopaminergic neurons
290 (TH^+) were identified using the same criteria as for $pS6^+$ neurons.

291 TH^+ nuclei groups were identified according to (Rink and Wullimann, 2001; Panula et al.,
292 2010; Parker et al., 2013) (Figure 4-1). We counted TH^+ cells in the following clusters: the
293 subpallium area (extending from the rostroventral telencephalon to the dorsocaudal
294 telencephalon, also identified as G2 by Panula and colleagues (Panula et al., 2010),
295 which included a TH cluster containing Vv, Vc and Vl, and in-between areas, a TH cluster
296 including Vd and the lateral area outside the Vd, and a TH cluster within the Vs (identified
297 by the anterior commissure) and lateral area outside the Vs; TH clusters in the PPa area
298 were divided in two: a more anterior (close to the border of the diencephalon, lateral
299 margin of the ventricle, G3) and a more posterior extending area in the medial area of the
300 PPa (ventral part of the PPa), G4); a TH cluster in the pretectum (PPr, G7); in the
301 ventromedial and ventrolateral nucleus (Vm, Vl, G6); a TH cluster in the periventricular
302 nucleus of the posterior tuberculum (TP/TP, small cells, ventral to the central posterior
303 thalamic nucleus (CP), G11) and in the posterior tuberal nucleus (PTN, G12) (Figure 4-
304 1). Similar to pS6 neuronal quantification described above, we manually analyzed five
305 coronal brain slices for each cluster, in each brain hemisphere, placing one square of
306 1000 μm^2 in the brain region of interest with the highest density of cells.

307 **Statistical analysis**

308 Data are represented as mean ± standard error of the mean (SEM). Normality of the data
309 was tested by D´Agostino and Pearson omnibus normality test and Shapiro-Wilk
310 normality tests. When parametric assumptions were verified, we used parametric
311 statistics; otherwise we used equivalent non-parametric tests, namely Mann-Whitney
312 tests to compare the effect of MTZ treatment on OXT mRNA, on the expression of the
313 NTR-mCherry transgene, and to compare the adult social affiliation score between
314 untreated and MTZ-treated groups at different developmental time points (4-6 days-old,
315 12-14 days-old, 22-24 days-old and 90 days-old MTZ-treatment). Significance was
316 denoted as $p < 0.05$, and p-values refer to two-tailed tests, unless otherwise noted. The
317 use of one-tailed tests was justified by a priori directionality hypotheses in the following
318 cases:

319 - Effect of MTZ treatment on OXT mRNA and NTR-mCherry transgene expression (Figure
320 2 and Figure 2-1), since in our system, we expected that MTZ would ablate the NTR-
321 oxytocinergic expressing neurons;

322 - Effect of MTZ treatment (oxytocinergic ablation) on social affiliation behavior in fish
323 expressing the NTR transgene, and thus causing OXT ablation, since OXT is well known
324 to regulate social behaviors and thus, we expected that oxytocinergic ablation would lead
325 to a decreased social behavior in zebrafish (Figure 2).

326 **Statistical analysis of behavioral data:** One sample *t*-tests were used to verify if social
327 affiliation during development was statistically different from chance (0.5). Because we
328 tested eight independent cohorts for the effect of MTZ-treatment at 4-6 days-old time point
329 (by different researchers in two different laboratories), the total sample size for this time
330 point (n=210) was much larger than for the other time points (12-14 days-old: n=28, 22-
331 24 days-old, n=19; adult: n=13). Taking in account all eight cohorts together, the adult
332 social affiliation score of the 4-6 days-old MTZ-treated fish were significantly decreased
333 from untreated siblings (p=0.0012, Mann-Whitney test, n= 112 untreated vs. 98 MTZ-
334 treated fish). However, a Generalized Linear Model (GLM) with beta regression and
335 planned comparisons, which was used to compare the effect of MTZ treatment on adult
336 social affiliation score of the eight different cohorts (Figure 2-3), revealed not only an
337 effect of the MTZ treatment (F_1=9.486, p=0.0021) but also variation among cohorts
338 (F_7=2.719, p=0.0081, Figure 2-4). We therefore performed a Monte Carlo simulation for
339 a sample size of 30 individuals sampled from the observed data, 15 individuals from each
340 group (untreated and 4-6 days-old MTZ treated) with 1000 iterations. This simulation,
341 ensured a more comparable sample size for the 4-6 days-old time point treatment relative
342 to other time-point treatments. Moreover, it ensured a more representative sample than
343 each cohort independently or the total eight-cohort population. We obtained a Monte
344 Carlo p-value of p<0.001 (Figure 2E), which means that there was a significantly higher
345 number of simulations in which the social affiliation score of the untreated group was
346 greater than the social affiliation score of the MTZ-treated group, as compared to the
347 number of simulations with the inverse trend, for a sample size of 15 individuals, across
348 all eight cohorts. P-value was calculated as the mean social affiliation score of the 1000

349 iterations for untreated fish divided by the mean scores of the 1000 iterations for treated
350 fish divided by 1000.

351 To determine whether the difference in social affiliation score between untreated and 4-6
352 days-old MTZ-treated fish was due to OXT ablation and not movement impairments
353 caused by MTZ, we used a Linear Model (LM) to compare the total distance moved
354 (square root transformed) of both groups in the eight independent cohorts. Both GLM with
355 beta regression on adult social affiliation score and LM on total distance moved (square
356 root transformed) were also applied to different control cohort fish not expressing NTR
357 transgene (Figure 2-3, 2-5). In all of these models (GLM and LM) the explanatory
358 variables were treatment and cohorts for mains effects and interaction.

359 **Statistical Analysis of neuronal activation (ps6 cell quantification):** To compare
360 neuronal activation between treatments and stimuli, we used a Generalized Linear Mixed
361 Model (GLMM) with a Poisson distribution using the brain identification number as the
362 random effect in the statistical model, followed by planned comparisons, since we target
363 areas that are known to belong to the social decision-making network. We checked
364 whether the data were normally distributed with Shapiro-Wilk tests for each brain area.
365 Since they were not, and because the data are counts, we checked the fit of the data to
366 the Poisson distribution with the "fitdistrplus" package from R (Delignette-Muller and
367 Dutang, 2015). By visual inspection of density and cumulative distribution plots we
368 validated that the Poisson distribution was the most appropriate to our data analyses. As
369 fixed effects we used treatment and stimuli. We analyzed the 16 brain areas
370 independently and corrected the p-values of the planned comparison with the false
371 discovery rate (FDR) adjustment method.

372 **Statistical Analysis of dopaminergic cell quantification:** To compare dopaminergic
373 cell numbers between treatments, and since the data were normally distributed (G7: W =
374 0.97685, p-value = 0.6383; G12: W = 0.9546, p-value = 0.1459; G2: W = 0.95265, p-
375 value = 0.1267; Shapiro-Wilk test), LM was performed to assess the effect of 4-6 days-
376 old MTZ-treatment in total TH counts of three distinct independently analyzed TH clusters
377 in 8 days-old larvae (Figure 3, 3-1).

The effect of 4-6 days-old MTZ treatment on adult dopaminergic system was also assessed with a GLMM with a Poisson regression followed by planned comparisons, comparing the number of TH-positive cells sampled in five squares of 1000 μm^2 per TH cluster in 8 different adult brain TH clusters. As fixed effects we used treatment and stimuli. All eight areas were analyzed independently and p-values of the planned comparisons were corrected with the FDR adjustment method (Figure 4 and 4-2).

Data analysis software: Graphical representations of the data were performed in GraphPad Prism 6.0c software. Shapiro-Wilk normality test, one-sample *t*-test and *t*-tests were performed in GraphPad Prism, and the remaining tests were performed in R programming software, version 3.6.3 (R_core_Team, 2013) with the following packages: lme4(Bates et al., 2015) and afex (Henrik Singmann, Ben Bolker, Jake Westfall, 2020) (for GLMM with Poisson regression), betareg (for GLMM with beta regression), emmeans (for planned comparisons)(Lenth, 2020), and the base R package (for LM regression and Monte Carlo simulations)(R_core_Team, 2013).

Functional connectivity analysis

Functional connectivity, which has been defined as the temporal coincidence of spatially distant neurophysiological events (Friston, 1994), is typically inferred from temporal correlations between distinct brain areas in human fMRI data from both resting state and task-state studies (Biswal et al., 1997). The rationale for this approach is that areas that show a consistent correlation in their activity are components of the same brain network. Therefore, the concept of functional connectivity is purely correlative in nature, and per se it does not imply a direct causal relationship or the occurrence of structural connectivity between the correlated brain areas (Eickhoff and Müller, 2015). Functional connectivity can also be inferred from correlations across subjects using the expression of molecular markers such as immediate early genes (Teles et al., 2015). Similarly, we computed functional connectivity for our neuronal activity data based on the co-expression of pS6 across different brain regions for the set of individuals of each experimental treatment. For this purpose we have developed the method described below, which statistically validates the identified networks.

Network reconstruction: To test for functional connectivity of early MTZ-treated vs untreated brains exposed to social stimuli, we reconstructed Pearson correlation matrices using a resampling procedure, similar to the Quadratic Assignment Procedure (QAP) (Makagon et al., 2012; Borgatti et al., 2013). Instead of defining a single network, we construct the set of possible networks obtained leaving out some of the specimens' information. More precisely, consider the case of M specimens, each with an associated expression vector $x_i \in \mathbb{R}^N$, where N is the number of brain regions. For a given $m < M$, we consider all the $\binom{M}{m}$ combinations Ω_γ of m specimens and compute the corresponding functional graphs. We refer to the collection of graphs obtained in this way as a graph tower Ω_Γ, where each of the combinations can be considered as a graph layer. The advantage of this construction is that each layer in the graph tower represents a different instance of the network bootstrapping. In this way, observables computable on a single layer can be bootstrapped across multiple ones. The construction has naturally one parameter, the sampling number m, which needs to be chosen on the basis of data-driven considerations. In our experiments, robustness analysis shows that results are robust for m values between 10 and 15. To obtained sparse functional connectivity matrices, we threshold each instance following (De Vico Fallani et al., 2017) at a density threshold of $\rho = 0.2$, which also corresponds to the minimum network heterogeneity across instances. After thresholding, for each treatment we average the thresholded instances to obtain a single matrix per treatment, which we use in the following analysis.

Detection of robust functional modules: Communities were computed using the Leiden community detection method (Traag et al., 2019) on the averaged treatment matrices. To increase the robustness of the detection, for each condition, we repeat the community detection 400 times. From the 400 candidate partitions we extract the central partition as described in (Peixoto, 2021) and associate the resulting central partition to the treatment under analysis. To quantitatively characterize differences among partitions, we measure the ratio r of total edge weights within a community with that of the edges between communities. More specifically, for a partition $\mathcal{P}$ with s communities we compute the $s \times s$ matrix P, defined as

$$P_{\alpha\beta} = \sum_{i \in \alpha, j \in \beta} \omega_{ij}$$

Where $\alpha, \beta = 0, \ldots m-1$ label the modules of $\mathcal{P}$ and ω_{ij} is the edge weight between regions i and j. We then compute the ratio of average intra-community to inter-community edge weights as follows:

$$r = \frac{(m-1)\sum_{\alpha} P_{\alpha\alpha}}{2\sum_{\alpha \neq \beta} P_{\alpha\beta}} =$$

$$\frac{(m-1)}{2} \frac{TrP}{|P|_1 - TrP}$$

which measures the ratio of the average weight on the diagonal of $P_{\alpha\beta}$ to the average diagonal weight. To assess significance of r values and of differences between them, we employ a permutation test based on permutating the community labels while preserving the size of the considered communities. We find that all r values are significantly different from zero, and so are also the differences in r between treatments ($p<0.01$).

Strength centrality: As a measure of local integration, we computed also the strength centralities. The first encodes how strongly a node links to its neighbors. while the second total measures how influential a node is at the network level on the basis of its direct connections and how well connected its neighbors are. In Figure 6-4 we report the nodes ranked in decreasing order of strength (weighted degree) centrality.

454 **RESULTS**

455 **Early life ablation of oxytocinergic neurons decreases social affiliation**

456 Zebrafish is a highly gregarious species exhibiting well-characterized social behaviors
457 (reviewed in (Nunes et al., 2017)). We quantified the visually-mediated motivation of
458 zebrafish to approach conspecifics, as an indicator of social affiliation, by performing a
459 two-choice preference test measuring the time that individuals spend either near a
460 compartment containing a shoal of conspecifics or an empty one (Ribeiro et al., 2020a,
461 2020b). When an adult zebrafish is visually presented with both shoal and non-shoal
462 compartments, in a side-by-side configuration, it will spend most of the time in association
463 with the shoal; however, if shoal is not visible, fish tend to explore the entire arena
464 (Figure1 A,B). In accordance with previous reports (Engeszer et al., 2007; Dreosti et al.,
465 2015), we found social affiliation is an acquired developmental trait that emerges after the
466 third week of life. This was observed both in zebrafish that were repeatedly exposed to
467 the social affiliation behavioral arena throughout development (12 days-old (d): p= 0.69,
468 n=15; 14d: p=0.91, n=14; 16d: p=0.73, n=15; 16d: p=0.88, n=17; 22d: p=0.049, n=12;
469 24d: p=0.07, n=18; 26d: p=0.01, n=17; 28d: p=0.057, n=13; 30d: p=0.17, n=8; 33d:
470 p<0.0001, n=14; 62d: p=0.002, n=10; one sample t-test vs. theoretical score of 0.5
471 indicating no preference, Figure 1C), and in zebrafish that were only exposed to the arena
472 once at a specific developmental time point to avoid habituation to the setup (12d: p=0.34,
473 n=16; 19d: p=0.48, n=18; 21d: p=0.85, n=6; 26d: p=0.76, n=10; 36d: p=0.0007, n=13;
474 90d: p<0.0001, n=24; one sample t-test vs. theoretical score of 0.5 indicating no
475 preference, Figure 1C).

476 Oxytocin (OXT) has long been known to regulate social behaviors across species
477 (Goodson, 2008) and it has been linked to neurodevelopmental disorders that impact
478 social behavior during development and adulthood (Pobbe et al., 2012; Hovey et al.,
479 2014). This makes OXT a good candidate system for investigating neurodevelopmental
480 processes linked to social development. To disentangle the organizational vs. activational
481 effects of OXT neurons in the acquisition of adult social affiliation, we used a transgenic
482 line, *Tg(oxt:Gal4;UAS:NTR-mCherry)*, to express nitroreductase (NTR) protein fused to

483 the mCherry reporter, in oxytocin neurons (Figure 1D,E). In the presence of the drug
484 metronidazole (MTZ), NTR produces cytotoxic metabolites, thereby allowing temporally
485 controlled ablation of OXT neurons at different developmental stages (Curado et al.,
486 2007, 2008). We confirmed the expression of the NTR-mcherry fusion protein in the OXT-
487 ergic neuronal population by co-localizing the *Tg(oxt:Gal4;UAS:NTR-mCherry)* with a
488 transgenic reporter *Tg(oxt:EGFP)* at different stages of development (8, 14, 24 and 90
489 days-old, Figure 1E).

490 In both mammals and fish, OXT is produced by specific cells in the preoptic
491 hypothalamus which can be classified as magnocellular or parvocellular, based on soma
492 size (Sawchenko and Swanson, 1982; Van den Dungen et al., 1982; Knobloch and
493 Grinevich, 2014; Grinevich et al., 2016). We and others have previously shown that
494 zebrafish magnocellular OXT cells are clustered in the anterior-dorsal portion of the cell
495 group, whereas the parvocellular neurons make up the more ventral part of the group
496 (Wircer et al., 2017; Wee et al., 2019). We observed that the NTR-mCherry protein was
497 prominently expressed in the most anterior-dorsal part of the preoptic area (Figure 1E),
498 thus it can be considered to localize mainly to magnocellular OXT neurons in both larvae
499 and adult zebrafish. These cells have been shown to project to ventral forebrain in fish
500 (Saito et al., 2004). Also, recent research in rats has shown that these magnocellular cells
501 project to several brains regions including hypothalamus, amygdala, lateral septum and
502 nucleus accumbens (Zhang et al., 2021), indicating that this projection pattern is
503 evolutionarily conserved. MTZ treatment at all time points was highly effective (>80%
504 decrease) at ablating NTR-mCherry-positive OXT neurons (Figure 2-1). To ensure proper
505 ablation of endogenous OXT-ergic cells following MTZ treatment, we also performed
506 fluorescent *in situ* hybridization with probes directed against *oxt* mRNA at 4-6 days-old,
507 12-14 days-old, 22-24 days-old and in the adult (Figure 2A-C and Figure 2-2). A significant
508 decrease in OXT-expressing cells was observed following MTZ treatment at all tested
509 ages ($p= 0.0024$ n=11/10, $p=0.0003$ n=7/7, $p=0.0011$ n=7/8, $p=0.0079$ n=5/4, for 4-6
510 days-old, 12-14 days-old, 22-24 days-old and adult ablation untreated/treated,
511 respectively, one tailed Mann-Whitney test, Figure 2A'-C' and Figure 2-2).

512 To assess the effects of temporal OXT neuronal ablation on adult social affiliation,
513 zebrafish were treated with MTZ at specific time-points during development (4-6, 12-14,
514 22-24 days-old) or post-puberty (90 days-old) and social affiliation was assessed in
515 adulthood in comparison to untreated siblings (Figure 2D). We analyzed the social
516 affiliation scores of eight independent cohorts in which OXT neurons were ablated at 4-6
517 days days-old and found that despite considerable variation among cohorts during the
518 test, there was a robust effect of MTZ treatment on adult social affiliation (cohorts: p=
519 0.0081; treatment: p=0.001, see Statistical analysis section for detailed statistics of the
520 Generalized Linear Model (GLM) with beta regression, Figure 2-3, Figure 2-4). MTZ
521 treatment did not affect overall fish locomotion as measured by the total distance traveled
522 during the trial (cohorts: p=8.342e-16, treatment: p=0.668, Linear Model (LM), Figure 2-
523 3, Figure 2-4). We also observed variation among control adult cohorts not expressing
524 NTR but treated or untreated with MTZ at 4-6 days-old, without a main effect of MTZ-
525 treatment on either social affiliation score (cohort: p=0.0001, MTZ-treatment: p=0.2653,
526 GLM with beta regression, Figure 2-3, Figure 2-5) or total distance moved (cohort: p<2e-
527 16, MTZ-treatment: p=0.1536, LM, Figure 2-3, Figure 2-5).

528 In view of the biological variability observed across cohorts, we further verified the
529 effect of early-life OXT-neuron ablation on social affiliation by utilizing a Monte Carlo (MC)
530 simulation where we randomly sampled 15 treated and 15 untreated 4-6 days-old larvae
531 from all 8 cohorts and repeated the procedure for 1000 iterations. This analysis also
532 clearly indicated an impairment of adult social affiliation (p<0.0001, one-tailed Mann-
533 Whitney test, Figure 2E, see Statistical analysis for details on MC), which was maintained
534 in 12-14 days-old MTZ-treated adult fish (p=0.034, n=14/14, one-tailed Mann-Whitney
535 test, Figure 2E).

536 In contrast to the deficit in social affiliation caused by early life MTZ treatment, ablation
537 of OXT neurons in either 22-24 days-old or 90+ days-old animals did not affect adult
538 social affiliation (22-24: p=0.1364, n=10/9 one-tailed Mann-Whitney test; Adults:
539 p=0.3566, n=6/7, one-tailed Mann-Whitney test, Figure 2E). This result coincides with the
540 observation that social affiliation is a developmentally acquired trait which is established
541 before the juvenile stage of development (Figure 1C and (Dreosti et al., 2015).

542 Taken together, these results show that early developmental ablation of OXT neurons
543 leads to a long-term deficit in social affiliation in adulthood, suggesting that OXT neurons
544 are involved in an early-life developmental process that is required for proper social
545 affiliation later in life.

546 **Early life OXT ablation leads to impairments in specific dopaminergic clusters**

547 Notably, although early-life OXT neuronal ablation induced an impairment in social
548 affiliation, we observed complete recovery of the OXT neural population by adulthood, as
549 ablated fish displayed normal counts of OXT-expressing NTR-mCherry transgene (4-6
550 days-old MTZ-treated (n=14) vs. untreated (n=15) adult zebrafish: p= 0.33, unpaired t-
551 test, Figure 2F-H). We verified this result, obtained from imaging of the NTR-mCherry
552 transgene, by fluorescent in situ to OXT mRNA in adult fish subjected to early-life ablation,
553 and found no significant difference from controls (MTZ-treated (n=4) vs. untreated (n=5)
554 adult zebrafish: p= 0.25, two-tailed Mann-Whitney U test, Figure 2-7). We performed a
555 time-course analysis for the OXT neural recovery and we found that already within 1
556 month (i.e. by 42 days-old) from the MTZ-treatment there is no discernible difference
557 between treated and control animals (8 days-old, p<0.0001, n=15/15; 12 days-old,
558 p<0.0001, n=13/7; 19 days-old, p<0.0001, n=10/9; 26 days-old, p=0.0048, n=12/11; 42
559 days-old, p=0.59, n=9/10; Unpaired t test with Welch's correction, Figure 2-6). This is in
560 line with previous work showing that zebrafish neurons are capable of regenerating
561 following lesions even in adulthood (Kizil et al., 2012). Conversely, animals in which OXT
562 neurons were ablated in adulthood displayed normal social drive (Figure 2E) despite the
563 fact that the ablated cell populations had not yet recovered by the time of the behavioral
564 testing (Figures 2C, 2-1).

565 We therefore hypothesized that the developmental organization of the dopaminergic
566 system that also regulates social affiliation, might have been affected by early OXT
567 ablation. Therefore, we examined whether early perturbation of the OXT neuronal system
568 affected specific tyrosine hydroxylase (TH)- positive DA-ergic neuronal clusters (Figures
569 3, 4 and 4-1), which in zebrafish are anatomically discernible from other TH-positive
570 catecholaminergic cells (Ma, 1994a, 1994b, 1997; Rink and Wullimann, 2001, 2002), and

571 whether these effects persist over the long term. We observed that already 24 hours after
572 ablation of OXT neurons at 4-6 days-old, there was a significant decrease in
573 dopaminergic neuronal counts in the pretectum (PrT; p=0.009, n=18/18, LM, Figure 3B,
574 Figure 3-1), and the large neurons of the posterior tuberculum (TP; p=0.0045, n=18/18,
575 LM, Figure 3C, Figure 3-1). In contrast, no differences were found in telencephalic DA
576 neurons of the ventral subpallium area (Figure 3-1). The pretectum is the teleostean
577 homologue of the superior colliculus, an area known to be involved in gaze control and
578 possibly attention in zebrafish (Antinucci et al., 2019) as well as in mammals (Krauzlis et
579 al., 2004). The posterior tuberculum is the source of the ascending DA system, which is
580 considered analogous to the mammalian ventral tegmental area (VTA) (Rink and
581 Wullimann, 2001), which is involved in reward and reinforcement (Morales and Margolis,
582 2017).

583 Unlike the ablated OXT cells, which recovered over time, the deficits in DA neurons
584 observed in early OXT-ablated larvae persisted through adulthood, as adult fish that had
585 been treated with MTZ between 4-6 days-old displayed a reduced number of TH-positive
586 DA cells in the PrT (p=0.005, n=7/7; Figure 4B, Figure 4-2, GLMM). Similarly, OXT
587 ablation caused a decrease in the DA-ergic neurons residing in two subdivisions of the
588 TP, the periventricular nucleus of the posterior tuberculum (TP) and the posterior tuberal
589 nucleus (PTN), which are distinguishable only in the adult (TP p= 0.025, n=7/7; PTN p=
590 0.005, n=7/7; Figure 4C-D, Figure 4-2, GLMM with Poisson regression, planned
591 comparisons and FDR corrections).

592 To demonstrate that at the time of their ablation, OXT neurons physically interact with
593 the affected DA neurons, we examined whether OXT neurons form synapses on DA-ergic
594 clusters of the PrT and TP (Figure 5). We employed a double transgenic line,
595 *Tg(oxt:Gal4;UAS:Sypb-EGFP)*, which genetically expresses the synaptic marker,
596 synaptophysin-GFP in OXT neurons (Anbalagan et al., 2019), and visualized synaptic
597 contacts onto TH positive DA-ergic neurons (Figure 5). To ensure that these are indeed
598 bona-fide OXT releasing synapses, we also co-stained these fish with an anti-OXT
599 antibody (Blechman et al., 2018; Anbalagan et al., 2019) (Figure 5C-D). We found OXT
600 projections forming multiple synapses onto the DA neurons of the PrT and the TP (Figure

601 5C,D1,D2). We also observed OXT cells directly abutting the TH-positive cells of the TP
602 (Figure 5D3,D4), raising the possibility that OXT affects nearby DA-ergic cells in a non-
603 synaptic manner as has been shown in other species (Ludwig and Leng, 2006; Son et
604 al., 2013). These results indicate that these two systems, DA and OXT, are already linked
605 at early developmental stages and that early ablation of OXT neurons irreversibly impairs
606 the development of subsets of DA neurons which are key for social affiliation later in life.

607 **Early-life ablation of oxytocinergic neurons leads to impaired social information**
608 **processing**

609 In view of these results, we next examined whether these long-lasting developmental
610 changes also manifested in the neural processing response to social stimuli in adults,
611 focusing on vertebrate social decision-making network and mesolimbic reward system
612 (O'Connell and Hofmann, 2011). To this end, early-life ablated (MTZ-treated at 4-6 days-
613 old) adult zebrafish were exposed to a single visual social stimulus (a shoal of
614 conspecifics comprised of 2 females and 2 males) or an empty tank for controls, for 10
615 minutes, and their forebrain neuronal activity state was analyzed by immunostaining of
616 phosphorylated ribosomal protein S6 (pS6), a known correlate for neuronal activation
617 ((Knight et al., 2012), Figure 6). We then quantified the number of pS6-positive neurons
618 in several specific brain areas known to be implicated in neural processing of social
619 information and social reward (O'Connell and Hofmann, 2011) (Figures 6, 6-1, 6-2).
620 Results showed that early OXT ablation significantly affected neuronal activity in
621 response to social stimulus in two specific areas: the anterior part of the parvocellular
622 preoptic nucleus (Ppa) and in the most anterior part of the ventral nucleus of ventral
623 telencephalon (Vv) (GLMM with Poisson regression, planned comparisons and false
624 discovery rate (FDR) corrections, Figures 6B-E, 6-2).

625 Specifically, we found that while unablated fish exhibited increased activity in the Ppa
626 upon exposure to a shoal of conspecifics, this was not observed in early ablated fish
627 (untreated shoal vs untreated empty, p= 0.024, n= 11/7 respectively; MTZ-treated shoal
628 vs MTZ-treated empty, p=0.88, n=10/6 respectively; Figure 6B,C, Figure 6-2). Vv neurons
629 of unablated fish exhibited decreased activity upon exposure to a social stimulus,

630 whereas early ablated animals maintained their neuronal activity regardless of the
631 stimulus (untreated shoal vs untreated empty, p= 0.024, n=11/7 respectively; MTZ-treated
632 shoal vs MTZ-treated empty, p=0.88, n= 11/7 respectively; Figure 6D,E; Figure 6-2).

633 These results show that these two brain areas display deficits in neuronal response to
634 a social stimulus in early OXT-ablated zebrafish. Importantly, the Vv is considered
635 analogous to the mammalian lateral septum (LS), while the Ppa is analogous to the
636 mammalian preoptic hypothalamus (POA) (Wullimann and Mueller, 2004; O'Connell and
637 Hofmann, 2011). These areas are core nodes of the social behavior network in all
638 vertebrate species and have a strong reciprocal connection with each other (Wullimann
639 and Mueller, 2004; O'Connell and Hofmann, 2011).

640 We next examined whether early-life ablation of OXT neurons in the POA altered
641 functional connectivity between forebrain nuclei belonging to the social decision-making
642 network (SDMN; (O'Connell and Hofmann, 2012)), by comparing the correlation matrices
643 of activity levels for the different areas between ablated and non-ablated fish in either
644 basal state or in response to social stimulus (Figure 6-3, 6-4). We constructed correlation
645 matrices corresponding to each treatment via a resampling scheme, inspired by
646 Quadratic Assignment Procedure (Makagon et al., 2012), that additionally allows to
647 choose the threshold for sparsification on the basis of minimal heterogeneity across
648 resampled correlation matrices (see Methods). To identify functional reconfigurations
649 between different treatments, we identified mesoscale differences in the way the
650 functional networks are organized by their modular (or community) structure. To extract
651 such modules, we performed community detection using the Leiden algorithm (Traag et
652 al., 2019) on the functional connectivity matrix of each treatment. To ensure the
653 robustness of the resulting partitions, we repeated the optimization 400 times per
654 treatment and reconciled the different candidate partitions by considering the central
655 partition (Peixoto, 2021) (see final partitions in Figure 6F). Already by visual inspection it
656 is possible to observe differences in the overall community structure between treatments
657 in the allocation of nodes to communities, and in the relative integration within and across
658 communities. We quantified such integration by calculating the ratio r of the total edge
659 weights within communities to the total edge weights between different communities (see

660 Methods). We found that in the basal state (i.e. when no visual stimulus was presented)
661 the mesoscale functional organization is different between ablated ($r = 4.6$) and non-
662 ablated fish ($r = 7.5$), implying that the ablation of OXT neurons in the POA modifies the
663 resting state networks of the forebrain SDMN (Figure 6F). In particular, ablated fish show
664 a much less segregated network with respect to non-ablated ones. Secondly, we
665 observed that, in response to the social stimulus (i.e. sight of a conspecific shoal), the
666 functional network of non-ablated fish transitions from a segregated state ($r = 7.5$) to a
667 more integrated one ($r = 3.7$), whereas ablated fish showed the opposite pattern, moving
668 from a more integrated basal state ($r = 4.6$) to a more segregated response network
669 ($r = 6.4$). All r values are significantly different from zero, and also significantly different
670 from each other ($p < 0.01$). Finally, we completed the network analysis focusing on local
671 differences in terms of network centralities. In particular, we looked at the strength of
672 nodes, representing how strongly a node is connected to its neighbors (Figure 6-4). We
673 found a strong and significant anti-correlation between the ranking of strengths for the
674 ablated versus non-ablated fish in response to the social stimulus (Untreated Shoal vs
675 MTZ-treated Shoal, Spearman r=-0.5, p=0.01), implying that the hub nodes for non-
676 ablated fish are poorly connected nodes for the ablated and vice versa. Specifically, in
677 untreated fish exposed to the social stimulus, the most connected nodes were the
678 posterio-ventral part of the ventral telencephalon (Vv_p), followed by the medial zone of
679 the dorsal telencephalic area (Dm), two regions that have been implicated in the
680 regulation of social interactions and motivated behavior in zebrafish (von Trotha et al.,
681 2014; Stednitz et al., 2018). In contrast, both these nodes drop their centrality in the
682 SDMN network of MTZ-treated fish exposed to the social stimulus (from 1st to 5th and from
683 2nd to 16th, among 16 nodes, respectively), where the anterio- dorsal part of the ventral
684 telencephalon (Vd_a) and the lateral part of the ventral telencephalon (Vl), two poorly
685 connected nodes in untreated fish (ranking 14th and 16th, out of 16 nodes, respectively),
686 were the most connected nodes (Figure 6-4).

687 These results indicate that early-life OXT ablation leads to blunted response to shoal-
688 induced changes in brain activity within specific nuclei (Vv and Ppa), and to a wide-

689 ranging alteration in network connectivity spanning several nuclei of the social decision-
690 making network in both basal state and in response to social stimulus.

691 Taken together, our results show that proper response to social stimuli depends on
692 orchestrated co-development of OXT and DA neurons. We show that during
693 development, OXT has important organizational effects. Early developmental
694 perturbation of OXT neurons led to reduced attraction towards conspecifics, impaired the
695 neurodevelopment of specific DA-ergic neurons, caused a blunted neural response to
696 social stimuli in the forebrain (Ppa and Vv), and altered the connectivity of the SDMN.

697 **DISCUSSION**

698 Previous research has implicated OXT in various developmental disorders that affect
699 social function in humans, have highlighted its importance in social behavior in animals,
700 and indicated the importance of its communication with other systems, such as DA,
701 serotonin and estrogen for proper social behavior (Heinrichs et al., 2009; Hovey et al.,
702 2014; Grinevich et al., 2015; Grinevich and Stoop, 2018; Rajamani et al., 2018). However,
703 there has been limited investigation into the mechanistic aspects of OXTs developmental
704 functions, and how they are linked to its well-described social roles.

705 Here we utilize temporally controlled perturbations of OXT-ergic cells at different
706 developmental timepoints during zebrafish life to show that OXT has a distinct
707 developmental function, namely to enable proper development of specific downstream
708 DA-ergic clusters known to be involved in visual attention gating and reward (O'Connell
709 and Hofmann, 2011; Antinucci et al., 2019). We also show that in animals where this
710 developmental process was perturbed, the response to social stimuli is affected, and the
711 tendency to shoal with conspecifics is reduced.

712 The developmentally affected DA-ergic clusters, namely the pretectum (superior
713 colliculus) and the TP (VTA) have been linked in other organisms to social functioning at
714 the level of behavior and, at the molecular level, to the OXT system. Thus, in primates
715 and humans, which like zebrafish are highly dependent on vision for gathering social
716 information, OXT receptors are expressed in the superior colliculus (Schorscher-Petcu et

717 al., 2009; Freeman et al., 2014a, 2014b, 2018), and OXT modulates the gaze and
718 oculomotor responses controlled by this nucleus (Leknes et al., 2013; Kret and De Dreu,
719 2017). This is also true of the VTA, where OXT receptors are expressed, which functions
720 to promote sociability (Hung et al., 2017). Notably, rhesus monkeys subjected to early
721 social deprivation displayed a reduction in DA neurons of the VTA (Martin et al., 1991),
722 and mouse KO of the autism-associated gene Nlgn3 resulted in impaired OXT signaling
723 in DA-ergic neurons and aberrant activity in the DA-ergic neurons of the VTA (Hörnberg
724 et al., 2020). This further shows how early perturbations to the OXT system can lead to
725 wide-ranging and varied effects on other socially relevant systems in the brain. Whether
726 the changes in DA-ergic neurons, caused the observed changes in social affiliation and
727 neural activity is yet to be directly tested.

728 In addition to the DA-ergic deficits, we show that in normal fish, neurons of the Ppa
729 (analogous to the mammalian VTA) respond to social stimuli by increased activity, while
730 neurons of the Vv (analogous to the mammalian LS) respond by reducing their activity.
731 In contrast, in developmentally perturbed animals these areas do not change their activity
732 following presentation of the stimulus. Interestingly, the OXTR in the mammalian LS have
733 been implicated in the regulation of social fear (Guzmán et al., 2013; Menon et al., 2018).
734 In zebrafish, the Vv/LS has been functionally associated with social affiliation, mainly
735 through its cholinergic neurons (Stednitz et al., 2018). However, it is interesting to note
736 that in many animal models (e.g. rodents, teleosts, and cartilaginous fish), including
737 zebrafish, the Vv/LS has been shown to contain mainly GABAergic neurons, and to be a
738 source of GABAergic input to the VTA, a putative homologue of the TP, encompassing
739 the TP and PTN, in zebrafish (O'Connell and Hofmann, 2011), and to the POA (O'Connell
740 and Hofmann, 2011; Vega-Quiroga et al., 2018). Thus, it is possible that the observed
741 reduced activity in Vv/LS corresponds to GABAergic neurons that project to the Ppa and
742 TP. These areas are core nodes of the social behavior network in all vertebrate species
743 and have a strong reciprocal connection with each other (Wullimann and Mueller, 2004;
744 O'Connell and Hofmann, 2011). This suggests that social stimuli could promote a
745 disinhibition in these target areas, which would be associated with the rewarding and/or
746 motivational component of social affiliation. As a corollary, in early-ablated animals, where
747 Vv activity remains high in response to social stimuli, the TP would remain inhibited, and

748 the rewarding component of social affiliation would be attenuated, leading to decreased
749 display of this behavior.

750 In addition, we show that the overall coactivation patterns of forebrain nuclei involved
751 in social processing are altered in developmentally perturbed animals, both at baseline
752 and following presentation of a social stimulus. In other words, we show that the
753 connectivity between the different nodes of the social decision-making network changes
754 as a result of early life OXT ablation. We submit that the proper maturation of this network
755 at the level of neural architecture is dependent on early-life signaling by OXT neurons.

756 In summary, our results demonstrate that OXT neurons are required for the
757 developmental acquisition of social affiliation and exert an organizational effect on DA-
758 ergic neuronal populations. Furthermore, our results suggest that this role involves
759 orchestrating the co-development and maturation of several brain systems, such as the
760 midbrain social visual processing and attention systems (the pretectum), social decision-
761 making areas in the forebrain and ascending dopamine centers associated with reward.
762 When the OXT-dependent developmental process is perturbed, neural responses to
763 social stimuli in these regions become compromised, important parts of the social
764 decision-making network fail to synchronize their activity, and eventually, the propensity
765 to spend time near a shoal of conspecifics is reduced.

766

Funding:

ARN was supported by a Short-Term EMBO fellowship (ASTF 420-2013), by the Weizmann´s Dean of Faculty postdoctoral fellowship at the Weizmann Institute, Israel, and by Fundação para a Ciência e Tecnologia (FCT; SFRH/BPD/93317/2013) at Instituto Gulbenkian de Ciência, Portugal. M.G., E.W. and J.B. were supported by Israel Science Foundation (#1511/16); United States-Israel Binational Science Foundation (#2017325); Sagol Institute for Longevity and Estate of Emile Mimran . G.L. is an incumbent of the Elias Sourasky Professorial Chair. This work was funded by the project LISBOA-01-0145-FEDER-030627 co-funded by the Programa Operational Regional de Lisboa (Lisboa 2020), through Portugal 2020 and the European Regional Development Fund (FEDER), and by the FCT/MCTES through national funds (PIDDAC).

Authors contributions:

ARN- Designed the research, performed experiments, analyzed data, wrote/revised manuscript; MG - Designed the research, performed experiments, analyzed data, wrote/revised manuscript; EW- Performed experiments; JB- Performed experiments; GP and MT- Performed network analysis; SAMV- Performed statistical analysis; GL- Designed the research, supervision, edited/revised manuscript; RO- Designed the research, supervision, edited/revised manuscript

787 **REFERENCES**

788 Anbalagan S, Blechman J, Gliksberg M, Gordon L, Rotkopf R, Dadosh T, Shimoni E,
789 Levkowitz G (2019) Robo2 regulates synaptic oxytocin content by affecting actin
790 dynamics. Elife 8:e45650.

791 Anbalagan S, Gordon L, Blechman J, Matsuoka RL, Rajamannar P, Wircer E, Biran J,
792 Reuveny A, Leshkowitz D, Stainier DYR, Levkowitz G (2018) Pituicyte Cues
793 Regulate the Development of Permeable Neuro-Vascular Interfaces. Dev Cell
794 47:711-726.e5.

795 Antinucci P, Folgueira M, Bianco IH (2019) Pretectal neurons control hunting behaviour.
796 Elife 8:e48114.

797 Bartz JA, Zaki J, Bolger N, Ochsner KN (2011) Social effects of oxytocin in humans:
798 context and person matter. Trends Cogn Sci 15:301–309.

799 Bates D, Mächler M, Bolker BM, Walker SC (2015) Fitting linear mixed-effects models
800 using lme4. J Stat Softw 67.

801 Biswal BB, Van Kylen J, Hyde JS (1997) Simultaneous assessment of flow and BOLD
802 signals in resting-state functional connectivity maps. NMR Biomed 10:165–170.

803 Blechman J, Amir-Zilberstein L, Gutnick A, Ben-Dor S, Levkowitz G (2011) The
804 metabolic regulator PGC-1α directly controls the expression of the hypothalamic
805 neuropeptide oxytocin. J Neurosci 31:14835–14840.

806 Blechman J, Anbalagan S, Matthews GG, Levkowitz G (2018) Genome Editing Reveals
807 Idiosyncrasy of CNGA2 Ion Channel-Directed Antibody Immunoreactivity Toward
808 Oxytocin. Front Cell Dev Biol 6:117.

809 Borgatti SP, Everett MG, Johnson JC (2013) Analyzing Social Networks. Beverley Hills,
810 CA: Sage Publications.

811 Borges AC, Pereira N, Franco M, Vale L, Pereira M, Cunha M V., Amaro A,
812 Albuquerque T, Rebelo M (2016) Implementation of a Zebrafish Health Program in
813 a Research Facility: A 4-Year Retrospective Study. Zebrafish 13:S115–S125.

814 Bowen MT, Neumann ID (2017) Rebalancing the Addicted Brain: Oxytocin Interference

815 with the Neural Substrates of Addiction. Trends Neurosci 40:691–708.

816 Curado S, Anderson RM, Jungblut B, Mumm J, Schroeter E, Stainier DYR (2007)
817 Conditional targeted cell ablation in zebrafish: a new tool for regeneration studies.
818 Dev Dyn 236:1025–1035.

819 Curado S, Stainier DYR, Anderson RM (2008) Nitroreductase-mediated cell/tissue
820 ablation in zebrafish: A spatially and temporally controlled ablation method with
821 applications in developmental and regeneration studies. Nat Protoc 3:948–954.

822 Davison JM, Akitake CM, Goll MG, Rhee JM, Gosse N, Baier H, Halpern ME, Leach
823 SD, Parsons MJ (2007) Transactivation from Gal4-VP16 transgenic insertions for
824 tissue-specific cell labeling and ablation in zebrafish. Dev Biol 304:811–824.

825 De Vico Fallani F, Latora V, Chavez M (2017) A Topological Criterion for Filtering
826 Information in Complex Brain Networks. PLOS Comput Biol 13:e1005305.

827 Delignette-Muller ML, Dutang C (2015) fitdistrplus: An R package for fitting distributions.
828 J Stat Softw 64:1–34.

829 Dölen G, Malenka RC (2014) The Emerging Role of Nucleus Accumbens Oxytocin in
830 Social Cognition. Biol Psychiatry 76:354–355.

831 Donaldson ZR, Young LJ (2008) Oxytocin, vasopressin, and the neurogenetics of
832 sociality. Science (80-) 322:900–904.

833 Dreosti E, Lopes G, Kampff AR, Wilson SW (2015) Development of social behavior in
834 young zebrafish. Front Neural Circuits 9:1–9.

835 Eickhoff SB, Müller V. (2015) Functional Connectivity. In: Brain Mapping (Toga AW, ed),
836 pp Pp. 187-201. Academic Press.

837 Engeszer RE, Barbiano LA DA, Ryan MJ, Parichy DM (2007) Timing and plasticity of
838 shoaling behaviour in the zebrafish, Danio rerio. Anim Behav 74:1269–1275.

839 Freeman SM, Inoue K, Smith AL, Goodman MM, Young LJ (2014a) The
840 neuroanatomical distribution of oxytocin receptor binding and mRNA in the male
841 rhesus macaque (Macaca mulatta). Psychoneuroendocrinology 45:128–141.

842 Freeman SM, Palumbo MC, Lawrence RH, Smith AL, Goodman MM, Bales KL (2018)

843 Effect of age and autism spectrum disorder on oxytocin receptor density in the
844 human basal forebrain and midbrain. Transl Psychiatry 8:257.

845 Freeman SM, Walum H, Inoue K, Smith AL, Goodman MM, Bales KL, Young LJ
846 (2014b) Neuroanatomical distribution of oxytocin and vasopressin 1a receptors in
847 the socially monogamous coppery titi monkey (Callicebus cupreus). Neuroscience
848 273:12–23.

849 Friston KJ (1994) Functional and effective connectivity in neuroimaging: A synthesis.
850 Hum Brain Mapp 2:56–78.

851 Gamer M, Zurowski B, Büchel C (2010) Different amygdala subregions mediate
852 valence-related and attentional effects of oxytocin in humans. Proc Natl Acad Sci U
853 S A 107:9400–9405.

854 Goodson JL (2008) Nonapeptides and the evolutionary patterning of sociality. Prog
855 Brain Res 170:3–15.

856 Grinevich V, Knobloch-Bollmann HS, Eliava M, Busnelli M, Chini B (2016) Assembling
857 the Puzzle: Pathways of Oxytocin Signaling in the Brain. Biol Psychiatry 79:155–
858 164.

859 Grinevich V, Sophie Knobloch-Bollmann H, Eliava M, Busnelli M, Chini B (2015)
860 Assembling the Puzzle: Pathways of Oxytocin Signaling in the Brain. Biol
861 Psychiatry 79:155–164.

862 Grinevich V, Stoop R (2018) Interplay between Oxytocin and Sensory Systems in the
863 Orchestration of Socio-Emotional Behaviors. Neuron 99:887–904.

864 Guastella AJ, Hickie IB (2016) Oxytocin Treatment, Circuitry, and Autism: A Critical
865 Review of the Literature Placing Oxytocin into the Autism Context. Biol Psychiatry
866 79:234–242.

867 Guzmán YF, Tronson NC, Jovasevic V, Sato K, Guedea AL, Mizukami H, Nishimori K,
868 Radulovic J (2013) Fear-enhancing effects of septal oxytocin receptors. Nat
869 Neurosci 16:1185–1187.

870 Hammock EAD (2015) Developmental perspectives on oxytocin and vasopressin.

871 Neuropsychopharmacology 40:24–42.

872 Heinrichs M, von Dawans B, Domes G (2009) Oxytocin, vasopressin, and human social
873 behavior. Front Neuroendocrinol 30:548–557.

874 Henrik Singmann, Ben Bolker, Jake Westfall FA and MSB-S (2020) afex: Analysis of
875 Factorial Experiments. R package version 0.27-2.

876 Hörnberg H, Pérez-Garci E, Schreiner D, Hatstatt-Burklé L, Magara F, Baudouin S,
877 Matter A, Nacro K, Pecho-Vrieseling E, Scheiffele P (2020) Rescue of oxytocin
878 response and social behaviour in a mouse model of autism. Nature 584:252–256.

879 Hovey D, Zettergren A, Jonsson L, Melke J, Anckarsäter H, Lichtenstein P, Westberg L
880 (2014) Associations between oxytocin-related genes and autistic-like traits. Soc
881 Neurosci 9:378–386.

882 Hung LW, Neuner S, Polepalli JS, Beier KT, Wright M, Walsh JJ, Lewis EM, Luo L,
883 Deisseroth K, Dölen G, Malenka RC (2017) Gating of social reward by oxytocin in
884 the ventral tegmental area. Science (80-) 357:1406–1411.

885 Insel TR, Shapiro LE (1992) Oxytocin receptor distribution reflects social organization in
886 monogamous and polygamous voles. Proc Natl Acad Sci U S A 89:5981–5985.

887 Johnson Z V., Walum H, Xiao Y, Riefkohl PC, Young LJ (2017) Oxytocin receptors
888 modulate a social salience neural network in male prairie voles. Horm Behav
889 87:16–24.

890 Jurek B, Neumann ID (2018) The oxytocin receptor: From intracellular signaling to
891 behavior. Physiol Rev 98:1805–1908.

892 Keebaugh AC, Young LJ (2011) Increasing oxytocin receptor expression in the nucleus
893 accumbens of pre-pubertal female prairie voles enhances alloparental
894 responsiveness and partner preference formation as adults. Horm Behav 60:498–
895 504.

896 Kizil C, Kaslin J, Kroehne V, Brand M (2012) Adult neurogenesis and brain regeneration
897 in zebrafish. Dev Neurobiol 72:429–461.

898 Knight ZA, Tan K, Birsoy K, Schmidt S, Garrison JL, Wysocki RW, Emiliano A, Ekstrand

899 MI, Friedman JM (2012) Molecular profiling of activated neurons by phosphorylated
900 ribosome capture. Cell 151:1126–1137.

901 Knobloch HS, Grinevich V (2014) Evolution of oxytocin pathways in the brain of
902 vertebrates. Front Behav Neurosci 8.

903 Krauzlis RJ, Liston D, Carello CD (2004) Target selection and the superior colliculus:
904 Goals, choices and hypotheses. In: Vision Research, pp 1445–1451.

905 Kret ME, De Dreu CKW (2017) Pupil-mimicry conditions trust in partners: Moderation by
906 oxytocin and group membership. Proc R Soc B Biol Sci 284.

907 Leknes S, Wessberg J, Ellingsen D-M, Chelnokova O, Olausson H, Laeng B (2013)
908 Oxytocin enhances pupil dilation and sensitivity to 'hidden' emotional expressions.
909 Soc Cogn Affect Neurosci 8:741–749.

910 Lenth R (2020) emmeans: Estimated Marginal Means, aka Least-Squares Means. R
911 package version 1.4.7.

912 Lorenzi E, Mayer U, Rosa-Salva O, Vallortigara G (2017) Dynamic features of animate
913 motion activate septal and preoptic areas in visually naïve chicks (Gallus gallus).
914 Neuroscience 354:54–68.

915 Love TM (2014) Oxytocin, motivation and the role of dopamine. Pharmacol Biochem
916 Behav 119:49–60.

917 Ludwig M, Leng G (2006) Dendritic peptide release and peptide-dependent behaviours.
918 Nat Rev Neurosci 7:126–136.

919 Lukas M, Toth I, Reber SO, Slattery DA, Veenema AH, Neumann ID (2011) The
920 neuropeptide oxytocin facilitates pro-social behavior and prevents social avoidance
921 in rats and mice. Neuropsychopharmacology 36:2159–2168.

922 Ma PM (1994a) Catecholaminergic systems in the zebrafish. II. Projection pathways
923 and pattern of termination of the locus coeruleus. J Comp Neurol 344:256–269.

924 Ma PM (1994b) Catecholaminergic systems in the zebrafish. I. Number, morphology,
925 and histochemical characteristics of neurons in the locus coeruleus. J Comp Neurol
926 344:242–255.

927 Ma PM (1997) Catecholaminergic systems in the zebrafish. III. organization and
928 projection pattern of medullary dopaminergic and noradrenergic neurons. J Comp
929 Neurol 381:411–427.

930 Machluf Y, Levkowitz G (2011) Visualization of mRNA expression in the zebrafish
931 embryo. Methods Mol Biol 714:83–102.

932 Makagon MM, McCowan B, Mench JA (2012) How can social network analysis
933 contribute to social behavior research in applied ethology? Appl Anim Behav Sci
934 138:152–161.

935 Martin LJ, Spicer DM, Lewis MH, Gluck JP, Cork LC (1991) Social deprivation of infant
936 rhesus monkeys alters the chemoarchitecture of the brain: I. Subcortical regions. J
937 Neurosci 11:3344–3358.

938 Menon R, Grund T, Zoicas I, Althammer F, Fiedler D, Biermeier V, Bosch OJ, Hiraoka
939 Y, Nishimori K, Eliava M, Grinevich V, Neumann ID (2018) Oxytocin Signaling in
940 the Lateral Septum Prevents Social Fear during Lactation. Curr Biol 28:1066-
941 1078.e6.

942 Meyer MP, Smith SJ (2006) Evidence from in vivo imaging that synaptogenesis guides
943 the growth and branching of axonal arbors by two distinct mechanisms. J Neurosci
944 26:3604–3614.

945 Miller T V., Caldwell HK (2015) Oxytocin during development: Possible organizational
946 effects on behavior. Front Endocrinol (Lausanne) 6:76.

947 Morales M, Margolis EB (2017) Ventral tegmental area: Cellular heterogeneity,
948 connectivity and behaviour. Nat Rev Neurosci 18:73–85.

949 Noonan LR, Continella G, Pedersen CA (1989) Neonatal administration of oxytocin
950 increases novelty-induced grooming in the adult rat. Pharmacol Biochem Behav
951 33:555–558.

952 Nunes AR, Carreira L, Anbalagan S, Blechman J, Levkowitz G, Oliveira RF (2020)
953 Perceptual mechanisms of social affiliation in zebrafish. Sci Rep 10:1–14.

954 Nunes AR, Ruhl N, Winberg S, Oliveira RF (2017) Social phenotypes in zebrafish. In:

955 The Rights and Wrongs of Zebrafish: Behavioral Phenotyping of Zebrafish, pp 95–
956 130. Springer International Publishing.

957 O'Connell LA, Hofmann HA (2011) The Vertebrate mesolimbic reward system and
958 social behavior network: A comparative synthesis. J Comp Neurol 519:3599–3639.

959 O'Connell LA, Hofmann HA (2012) Evolution of a vertebrate social decision-making
960 network. Science (80-) 336:1154–1157.

961 Panula P, Chen YC, Priyadarshini M, Kudo H, Semenova S, Sundvik M, Sallinen V
962 (2010) The comparative neuroanatomy and neurochemistry of zebrafish CNS
963 systems of relevance to human neuropsychiatric diseases. Neurobiol Dis 40:46–57.

964 Park MJ, Seo BA, Lee B, Shin HS, Kang MG (2018) Stress-induced changes in social
965 dominance are scaled by AMPA-type glutamate receptor phosphorylation in the
966 medial prefrontal cortex. Sci Rep 8:15008.

967 Parker MO, Brock AJ, Walton RT, Brennan CH (2013) The role of zebrafish (Danio
968 rerio) in dissecting the genetics and neural circuits of executive function. Front
969 Neural Circuits 7:63.

970 Peixoto TP (2021) Revealing Consensus and Dissensus between Network Partitions.
971 Phys Rev X 11:021003.

972 Phoenix CH, Goy RW, Geral AA, Young WC (1959) Organizing action of prenatally
973 administered testosterone propionate on the tissues mediating mating behavior in
974 the female guinea pig. Endocrinology 65:369–382.

975 Pobbe RLH, Pearson BL, Defensor EB, Bolivar VJ, Young WS, Lee H-J, Blanchard DC,
976 Blanchard RJ, Blanchard RJ (2012) Oxytocin receptor knockout mice display
977 deficits in the expression of autism-related behaviors. Horm Behav 61:436–444.

978 R_core_Team (2013) R: A language and environment for statistical computing.

979 Rajamani KT, Wagner S, Grinevich V, Harony-Nicolas H (2018) Oxytocin as a
980 Modulator of Synaptic Plasticity: Implications for Neurodevelopmental Disorders.
981 Front Synaptic Neurosci 10:17.

982 Ribeiro D, Nunes AR, Gliksberg M, Anbalagan S, Levkowitz G, Oliveira RF (2020a)

983 Oxytocin receptor signalling modulates novelty recognition but not social
984 preference in zebrafish. J Neuroendocrinol 32:e12834.

985 Ribeiro D, Nunes AR, Teles M, Anbalagan S, Blechman J, Levkowitz G, Oliveira RF
986 (2020b) Genetic variation in the social environment affects behavioral phenotypes
987 of oxytocin receptor mutants in zebrafish. Elife 9:e56973.

988 Rink E, Wullimann MF (2001) The teleostean (zebrafish) dopaminergic system
989 ascending to the subpallium (striatum) is located in the basal diencephalon
990 (posterior tuberculum). Brain Res 889:316–330.

991 Rink E, Wullimann MF (2002) Connections of the ventral telencephalon and tyrosine
992 hydroxylase distribution in the zebrafish brain (Danio rerio) lead to identification of
993 an ascending dopaminergic system in a teleost. In: Brain Research Bulletin, pp
994 385–387.

995 Robinson KJ, Bosch OJ, Levkowitz G, Busch KE, Jarman AP, Ludwig M (2019) Social
996 creatures: Model animal systems for studying the neuroendocrine mechanisms of
997 social behaviour. J Neuroendocrinol 31:e12807.

998 Saito D, Komatsuda M, Urano A (2004) Functional organization of preoptic vasotocin
999 and isotocin neurons in the brain of rainbow trout: Central and neurohypophysial
1000 projections of single neurons. Neuroscience 124:973–984.

1001 Sallinen V, Torkko V, Sundvik M, Reenilä I, Khrustalyov D, Kaslin J, Panula P (2009)
1002 MPTP and MPP+ target specific aminergic cell populations in larval zebrafish. J
1003 Neurochem 108:719–731.

1004 Sawchenko PE, Swanson LW (1982) Immunohistochemical identification of neurons in
1005 the paraventricular nucleus of the hypothalamus that project to the medulla or to
1006 the spinal cord in the rat. J Comp Neurol 205:260–272.

1007 Schindelin J, Arganda-Carreras I, Frise E, Kaynig V, Longair M, Pietzsch T, Preibisch S,
1008 Rueden C, Saalfeld S, Schmid B, Tinevez JY, White DJ, Hartenstein V, Eliceiri K,
1009 Tomancak P, Cardona A (2012) Fiji: An open-source platform for biological-image
1010 analysis. Nat Methods 9:676–682.

1011 Schorscher-Petcu A, Dupré A, Tribollet E (2009) Distribution of vasopressin and

1012 oxytocin binding sites in the brain and upper spinal cord of the common marmoset.
1013 Neurosci Lett 461:217–222.

1014 Shamay-Tsoory SG, Abu-Akel A (2016) The Social Salience Hypothesis of Oxytocin.
1015 Biol Psychiatry 79:194–202.

1016 Son SJ, Filosa JA, Potapenko ES, Biancardi VC, Zheng H, Patel KP, Tobin VA, Ludwig
1017 M, Stern JE (2013) Dendritic peptide release mediates interpopulation crosstalk
1018 between neurosecretory and preautonomic networks. Neuron 78:1036–1049.

1019 Stednitz SJ, McDermott EM, Ncube D, Tallafuss A, Eisen JS, Washbourne P (2018)
1020 Forebrain Control of Behaviorally Driven Social Orienting in Zebrafish. Curr Biol
1021 28:2445-2451.e3.

1022 Tay TL, Ronneberger O, Ryu S, Nitschke R, Driever W (2011) Comprehensive
1023 catecholaminergic projectome analysis reveals single-neuron integration of
1024 zebrafish ascending and descending dopaminergic systems. Nat Commun 2:171.

1025 Teles MC, Almeida O, Lopes JSJSJS, Oliveira RF (2015) Social interactions elicit rapid
1026 shifts in functional connectivity in the social decision-making network of zebrafish.
1027 Proc R Soc B 282:20151099.

1028 Traag VA, Waltman L, van Eck NJ (2019) From Louvain to Leiden: guaranteeing well-
1029 connected communities. Sci Rep 9:1–12.

1030 Van den Dungen HM, Buijs RM, Pool CW, Terlou M (1982) The distribution of vasotocin
1031 and isotocin in the brain of the rainbow trout. J Comp Neurol 212:146–157.

1032 Vega-Quiroga I, Yarur HE, Gysling K (2018) Lateral septum stimulation disinhibits
1033 dopaminergic neurons in the antero-ventral region of the ventral tegmental area:
1034 Role of GABA-A alpha 1 receptors. Neuropharmacology 128:76–85.

1035 von Trotha JW, Vernier P, Bally-Cuif L (2014) Emotions and motivated behavior
1036 converge on an amygdala-like structure in the zebrafish. Eur J Neurosci 40:3302–
1037 3315.

1038 Wee CL, Nikitchenko M, Wang WC, Luks-Morgan SJ, Song E, Gagnon JA, Randlett O,
1039 Bianco IH, Lacoste AMB, Glushenkova E, Barrios JP, Schier AF, Kunes S, Engert

1040 F, Douglass AD (2019) Zebrafish oxytocin neurons drive nocifensive behavior via
1041 brainstem premotor targets. Nat Neurosci 22:1477–1492.

1042 Wircer E, Blechman J, Borodovsky N, Tsoory M, Nunes AR, Oliveira RF, Levkowitz G
1043 (2017) Homeodomain protein otp affects developmental neuropeptide switching in
1044 oxytocin neurons associated with a long-term effect on social behavior. Elife
1045 6:e22170.

1046 Wullimann MF, Mueller T (2004) Teleostean and mammalian forebrains contrasted:
1047 Evidence from genes to behavior. J Comp Neurol 475:143–162.

1048 Wullimann MF, Rupp B, Reichert H (1996) Neuroanatomy of the Zebrafish Brain.
1049 Birkhäuser Basel.

1050 Zhang B, Qiu L, Xiao W, Ni H, Chen L, Wang F, Mai W, Wu J, Bao A, Hu H, Gong H,
1051 Duan S, Li A, Gao Z (2021) Reconstruction of the Hypothalamo-Neurohypophysial
1052 System and Functional Dissection of Magnocellular Oxytocin Neurons in the Brain.
1053 Neuron 109:331-346.e7.

1054

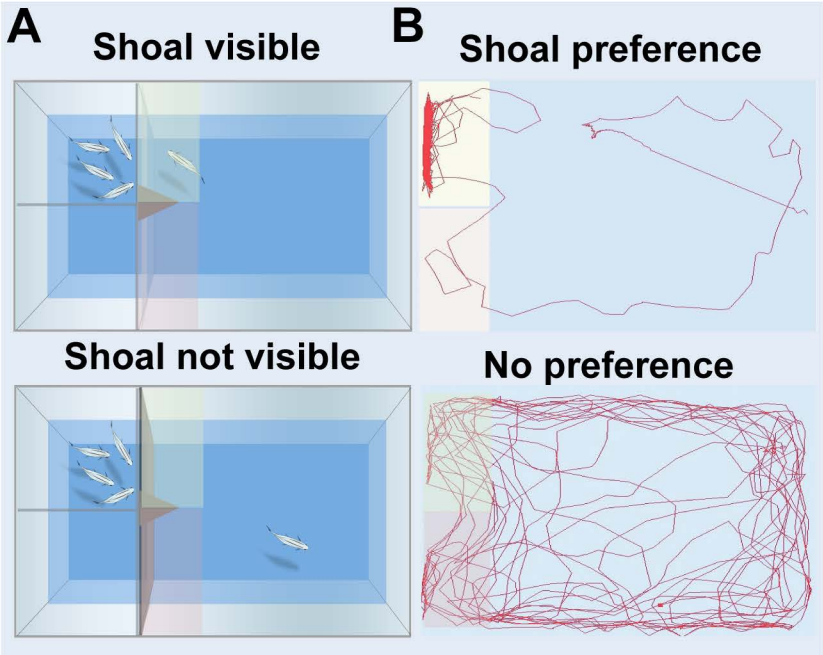
A
Shoal visible
B
Shoal preference
Shoal not visible
No preference

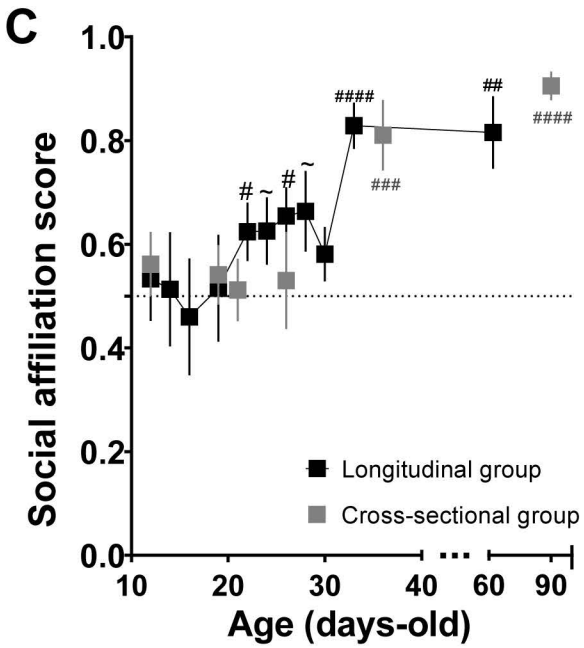
C
Social affiliation score
1.0
0.8
0.6
0.4
0.2
0.0
10
20
30
40
60
90
Age (days-old)
Longitudinal group
Cross-sectional group
#
~
#
~
####
###
##
####

D
oxt-p650
Gal4
x
UAS
NTR-mCherry

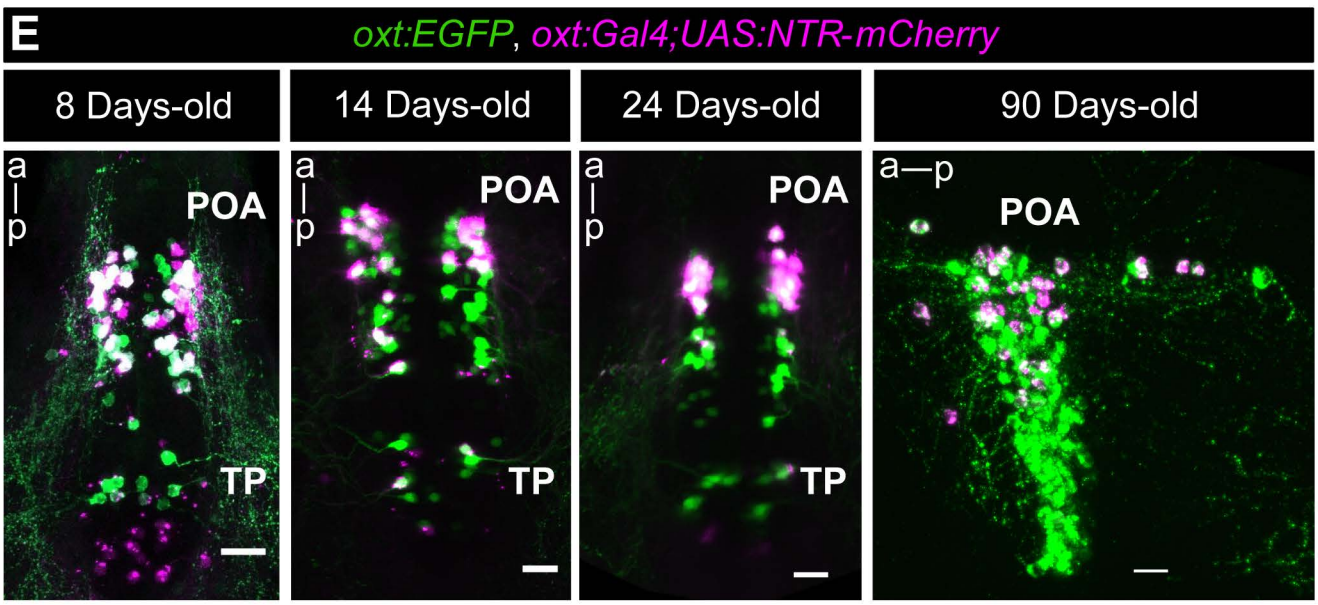
E
oxt:EGFP, oxt:Gal4;UAS:NTR-mCherry
8 Days-old
14 Days-old
24 Days-old
90 Days-old
a
p
POA
TP
a—p

Legends to Figures

Figure 1. Behavioral and genetic tools to study the role of oxytocinergic neurons in adult social affiliation. (A,B) Schematic representation of the visual-mediated shoal preference behavioral test setup. (A) When a mixed-sex shoal stimulus is visible, focal fish spends most of the time near the shoal (top). When the shoal is not visible (bottom), the focal fish explores the entire arena equally. (B) Representative tracking of the focal fish behavior. (C) Ontogeny of social affiliation in zebrafish. Visual preference to associate with a shoal of conspecific fish (social affiliation score> 0.5) emerges after the third week of life. Social affiliation score = $\%T_{shoal}/(\%T_{shoal} + \%T_{non\text{-}shoal})$. # Hash indicates a significant preference towards conspecifics, determined by a one-sample *t*-test with a hypothesized value of 0.5 (chance level). Fish were tested either repeatedly throughout development (black squares, longitudinal group) or only once at certain developmental time points (grey squares, cross-sectional group). (D) Spatio-temporal control of oxytocin-specific transgene expression. *oxt*:Gal4 drives the expression of nitroreductase tagged with mCherry fluorescent protein (NTR-mCherry) in oxytocinergic neurons. (E) *Tg(oxt:Gal4;UAS:NTR-mCherry)* characterization: NTR-mCherry+ cells co-localized with a subpopulation of *oxt*:eGFP neurons, at all developmental stages studied (8, 14 and 24 days-old: whole-mount larvae confocal z-stack image, dorsal view, anterior to top; 90 days-old, close-up of the preoptic area (POA), sagittal brain slice, confocal z-stack image, anterior to left).

Scale: 20 µm. TP, Posterior Tuberculum; POA, Preoptic area. Data presented as mean ± SEM.

# $p<0.05$, ## $p<0.01$, ### $p<0.001$, #### $p<0.0001$ (black # relates to the longitudinal group, grey # relates to the cross-sectional group).

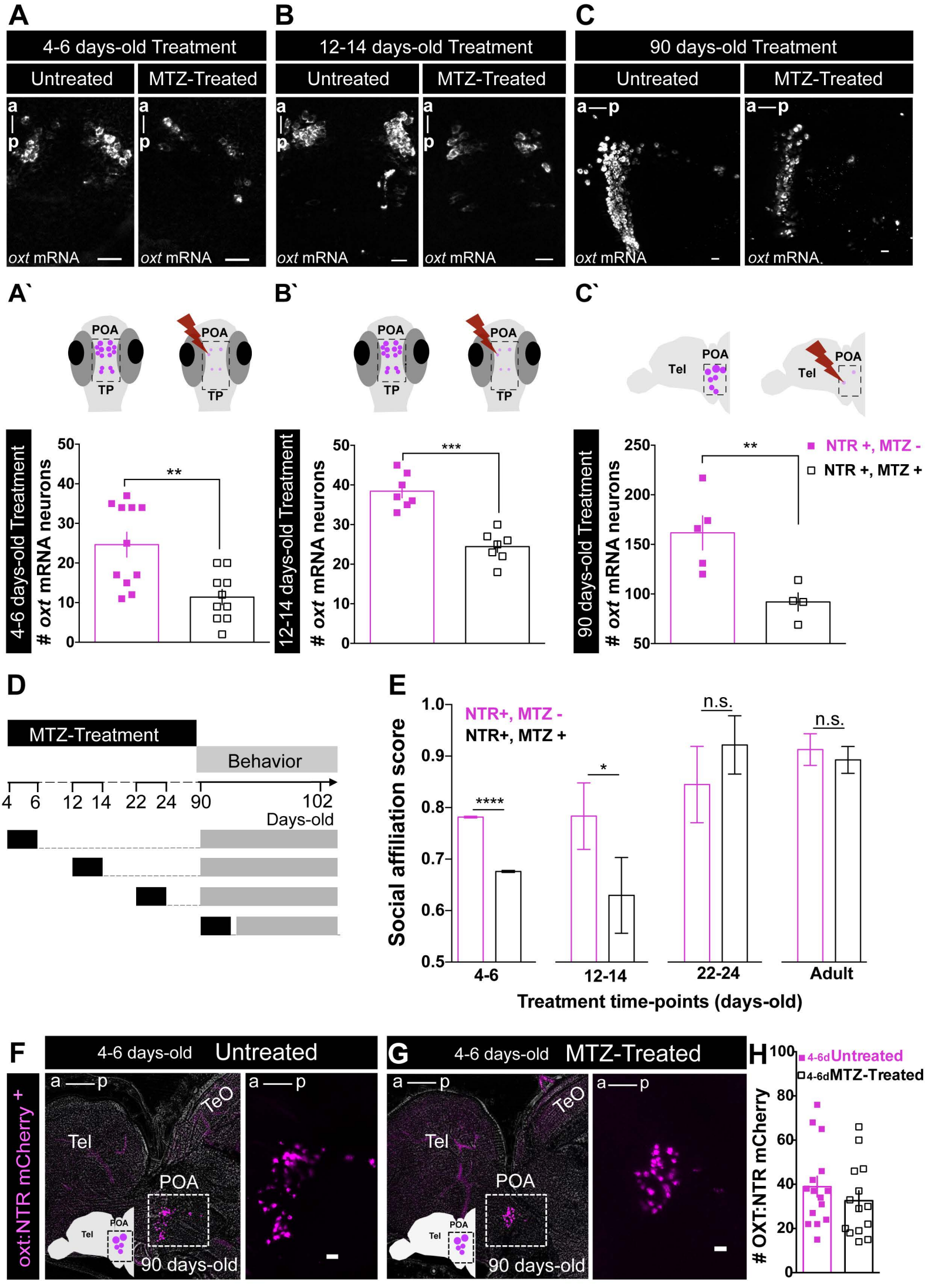
A
4-6 days-old Treatment
Untreated
MTZ-Treated
a
p
oxt mRNA
B
12-14 days-old Treatment
Untreated
MTZ-Treated
C
90 days-old Treatment
Untreated
MTZ-Treated
a—p
A`
B`
C`
POA
TP
Tel
4-6 days-old Treatment
12-14 days-old Treatment
90 days-old Treatment
oxt mRNA neurons
**
***
NTR +, MTZ -
NTR +, MTZ +
D
MTZ-Treatment
Behavior
4 6 12 14 22 24 90 102
Days-old
E
Social affiliation score
NTR+, MTZ -
NTR+, MTZ +
****
*
n.s.
n.s.
4-6
12-14
22-24
Adult
Treatment time-points (days-old)
F
4-6 days-old Untreated
oxt:NTR mCherry +
TeO
Tel
POA
90 days-old
G
4-6 days-old MTZ-Treated
H
4-6d Untreated
4-6d MTZ-Treated
OXT:NTR mCherry

Figure 2. Contrasting organizational vs activational effects of oxytocin neurons in adult social affiliation. (A-C) Representative examples of the effects of metronidazole (MTZ)- induced ablation on endogenous OXT as detected by *in situ* hybridization, at different treatment time-points. (A) 4-6 days-old treatment and (B) 12-14 days-old treatment: whole-mount larvae confocal maximum intensity z-stack image, dorsal view, anterior to top; (C) 90 days-old treatment: sagittal brain slice, confocal maximum intensity z-stack image, anterior to left. (A´-C´) Quantification of the number of cells expressing OXT mRNA in untreated fish or following MTZ treatment at: (A´) 4-6 days-old treatment, (B´) 12-14 days-old treatment and (C´) 90 days-old treatment. (D) Experimental timeline: fish were MTZ-treated at different developmental stages, allowed to grow until adulthood and then tested for social affiliation. (E) MTZ treatments during the first two weeks of life affect adult social affiliation. Social affiliation score = $\%T_{shoal} / (\%T_{shoal} + \%T_{non\text{-}shoal})$. Eight independent cohorts were treated at 4-6 days-old, and only one cohort at later time points. Therefore, in order to obtain comparable sample sizes among the different age-treatment groups and a more representative sample, the data for 4-6 days-old MTZ treatment shown in this graph were generated by a Monte Carlo simulation with 1000 iterations of samples of 15 individuals of each group (4-6 days-old MTZ-treated vs. untreated; see Statistical analysis subsection for details). One-tailed p-values were used because there was an *a priori* directional hypothesis that MTZ-treatment would ablate OXT neurons in fish expressing the NTR transgene and induce a decrease in social affiliation behavior. (F-H) OXT neurons ablated at 4-6 days-old were recovered by adulthood. (F) Representative example of NTR-mCherry-expressing OXT neurons in untreated adult fish. (G) Representative example of NTR-mCherry-expressing OXT neurons in adult fish treated with MTZ at 4-6 days-old. Images in (F,G) are maximum intensity confocal z-stacks, sagittal slices, anterior to left. (H) Quantification of the number of NTR-mCherry cells in untreated (full squares) and 4-6 days-old MTZ-treated adult fish (empty squares). Scale: 20 µm. Data presented as mean ± SEM. Full squares: untreated fish (NTR+, MTZ); Open squares: MTZ-treated fish (NTR+, MTZ+).

*$p<0.05$, **$p<0.01$,*** $p<0.001$. ****$p<0.0001$.

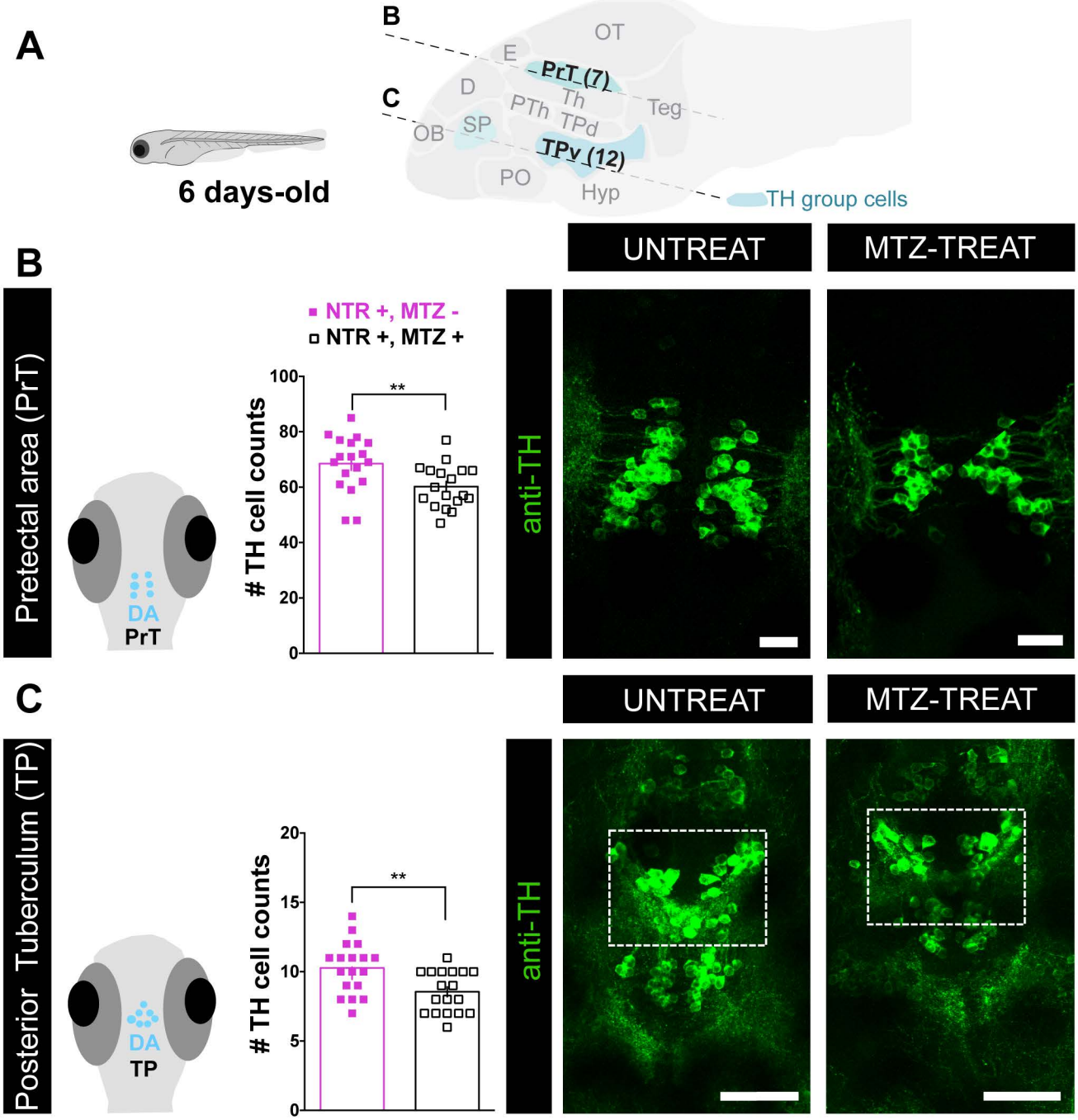
A
6 days-old
B
C
OT
E
PrT (7)
D
Th
PTh
TPd
Teg
OB
SP
TPv (12)
PO
Hyp
TH group cells
B
UNTREAT
MTZ-TREAT
Pretectal area (PrT)
NTR +, MTZ -
NTR +, MTZ +
TH cell counts
100
80
60
40
20
0
**
DA
PrT
anti-TH
C
UNTREAT
MTZ-TREAT
Posterior Tuberculum (TP)
TH cell counts
20
15
10
5
0
**
DA
TP
anti-TH

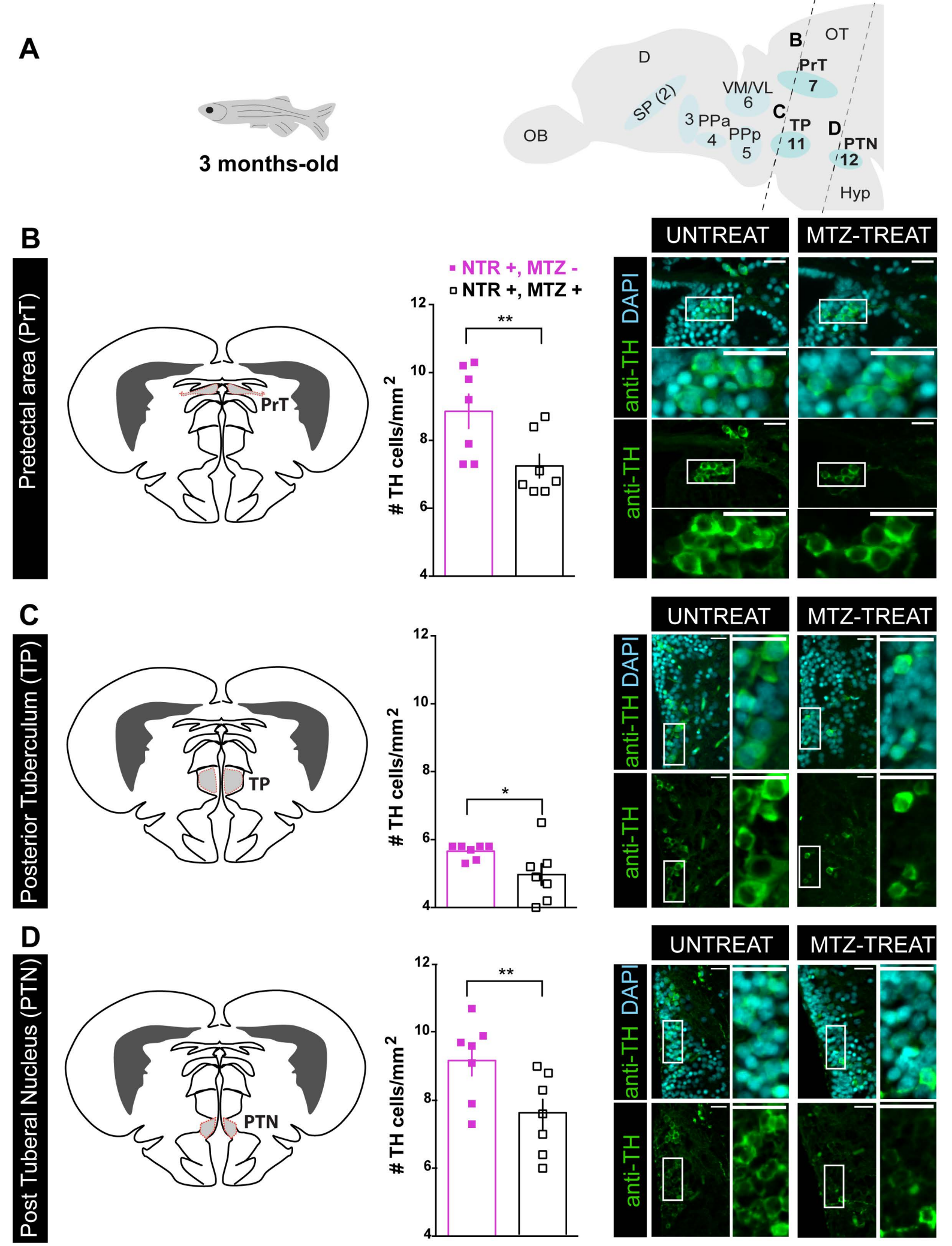
A
3 months-old
D
OB
SP (2)
3 PPa
4
VM/VL
6
PPp
5
B
OT
PrT
7
C
TP
11
D
PTN
12
Hyp
B
Pretectal area (PrT)
PrT
NTR +, MTZ -
NTR +, MTZ +
TH cells/mm2
**
UNTREAT
MTZ-TREAT
DAPI
anti-TH
C
Posterior Tuberculum (TP)
TP
*
D
Post Tuberal Nucleus (PTN)
PTN
**

Figure 3. Early-life OXT ablation affects the dopaminergic system in early development. (A) Top: Schematic sagittal section through a zebrafish larva brain showing the three dopaminergic clusters that were analyzed in this study, and highlighting two key dopaminergic brain areas that were affected by OXT neuronal ablation at 4-6 days-old, namely the pretectum (PrT) and posterior tuberculum (TP). Schematic was adapted from *zebrafishucl.org/forebrain-regions/posterior-tuberculum*. (B) Quantification of total pretectum (PrT) TH cell counts in untreated (NTR+, MTZ-) vs 4-6 days-old MTZ-treated (NTR+, MTZ+) larvae and respective representative images. Scale: 20 µm. (C) Quantification of total Posterior Tuberculum (TP) TH cell counts in untreated (NTR+, MTZ-) vs 4-6 days-old MTZ-treated (NTR+, MTZ+) larvae and respective representative images. Scale: 50 µm

. Data presented as mean ± SEM. Full squares: untreated fish (NTR+, MTZ); Open squares: MTZ-treated fish (NTR+, MTZ+).

*p<0.05, **p<0.01,*** p<0.001. ****p<0.0001.

D, dorsal telencephalon; *E*, epiphysis; *OB*, olfactory bulb; *OT*, optic tectum; *PO*, preoptic area; *PrT*, pretectum; *TPd*, posterior tuberculum dorsal part; *PTh*, prethalamus; *TPv*, posterior tuberculum ventral part; *Teg*, tegmentum; *Th*, thalamus; *SP*, subpallium (includes Vv, Vd and Vs in adult); *Hyp*, hypothalamus; *NTR*, nitroreductase; *MTZ*, metronidazole.

Figure 4. Early-life OXT ablation affects the dopaminergic system in adulthood. (A) Schematic sagittal section through a zebrafish adult brain, showing the eight dopaminergic clusters analyzed in this study, and highlighting the areas that were affected by OXT neuronal ablation at 4-6 days-old: Pretectal area (PrT), Posterior Tuberculum (TP) and Posterior Tuberal Nucleus (PTN). Dopaminergic groups are named according to (Panula et al., 2010; Parker et al., 2013). (B-D) Quantification of TH cell density (cells/mm^2; mean of five sampled slices for each area, see Methods section for details) in brains of adult fish untreated (NTR+, MTZ-) or MTZ-treated at 4-6 days-old (NTR+, MTZ+) and respective representative images in: (B) Pretectal area (PrT), (C) Posterior Tuberculum (TP) and (D) Posterior Tuberal Nucleus (PTN)

Scale: 20 μm. Data presented as mean ± SEM. Full squares: untreated fish (NTR+, MTZ); Open squares: MTZ-treated fish (NTR+, MTZ+).

*p<0.05, **p<0.01,*** p<0.001. ****p<0.0001.

D, dorsal telencephalon; *OB*, olfactory bulb; *OT*, optic tectum; *PrT*, pretectum; *TP*, posterior tuberculum; *SP*, subpallium (includes Vv, Vd and Vs); *Ppa*, anterior parvocellular preoptic nucleus; *VM*, ventromedial thalamic nucleus; *Vl*, ventrolateral thalamic nucleus; *PPp*, posterior parvocellular preoptic nucleus; *PTN*, posterior tuberal nucleus; *Hyp*, hypothalamus; *NTR*, nitroreductase; *MTZ*, metronidazole.

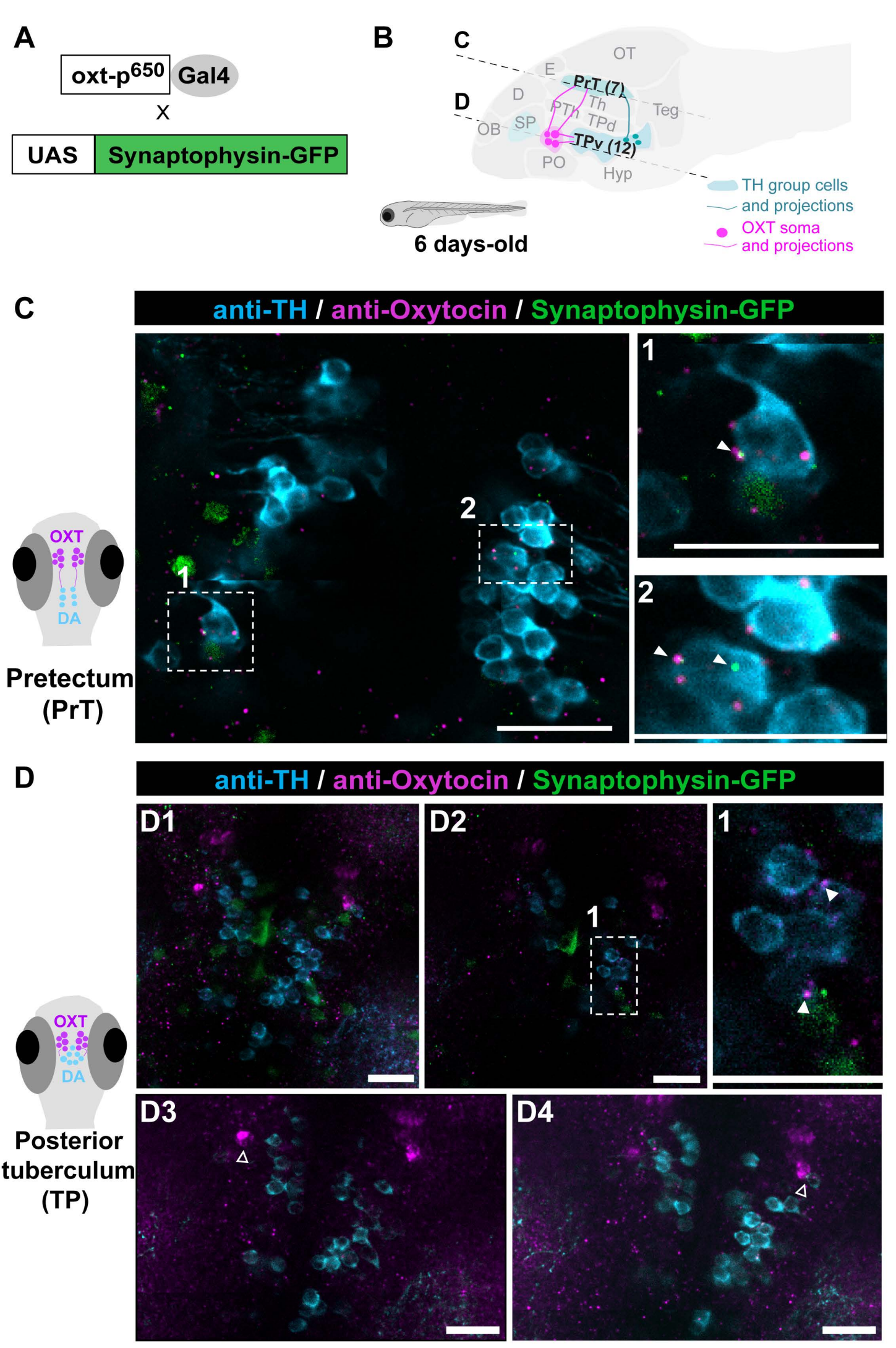
A
oxt-p650
Gal4
X
UAS
Synaptophysin-GFP
B
C
D
OT
E
PrT (7)
D
Th
PTh
TPd
Teg
OB
SP
TPv (12)
PO
Hyp
TH group cells
and projections
OXT soma
and projections
6 days-old
C
anti-TH / anti-Oxytocin / Synaptophysin-GFP
1
2
OXT
DA
Pretectum
(PrT)
D
anti-TH / anti-Oxytocin / Synaptophysin-GFP
D1
D2
D3
D4
OXT
DA
Posterior
tuberculum
(TP)

Figure 5. OXT neurons project to pretectal and posterior tuberculum dopaminergic clusters. (A) OXT neuron-specific labeling of synapses: *oxt*:Gal4 drives the expression of the EGFP-fused synaptic vesicle marker synaptophysin-B in oxytocinergic synapses. (B) Schematic of a sagittal larva brain highlighting OXT neuronal projections (in magenta) to pretectal and posterior tuberculum dopaminergic clusters (in blue). (C-D) Representative example showing that the synaptic marker line synaptophysin-GFP (green), driven under the OXT promoter, reveals bona fide OXT synapses containing the OXT peptide (anti-OXT, magenta) on TH positive cells (cyan) in both (C) pretectum (scale: 10 µm) and (D1-D2) posterior tuberculum clusters (scale: 20 µm). (D1) Optical projection overview of the posterior tuberculum. (D2) Single plane image. 1 and 2 depicts amplifications of the OXT synapses on TH positive cells in (C) pretectum and (D2) posterior tuberculum. Closed arrowheads point to OXT positive synaptophysin positive synapses that are in direct contact with TH cells. (D3-D4) 6 slice projection (total 6 µm thickness) of two different planes (scale: 20 µm). Open arrowheads indicate OXT neuron abutting the TH cells of the posterior Tuberculum. Images taken with Zeiss Ism 810 confocal scanning microscope, scaling (x*y*z)= 0.156*0.156*0.96 (µm/pixel), pinhole=31µm, Plan Apochromat 20X/0.8 M27 objective, excitation lasers: green channel (syn-GFP)-488nm; teal (anti-TH) channel-561 nm; magenta (anti-OXT) channel- 640 nm).

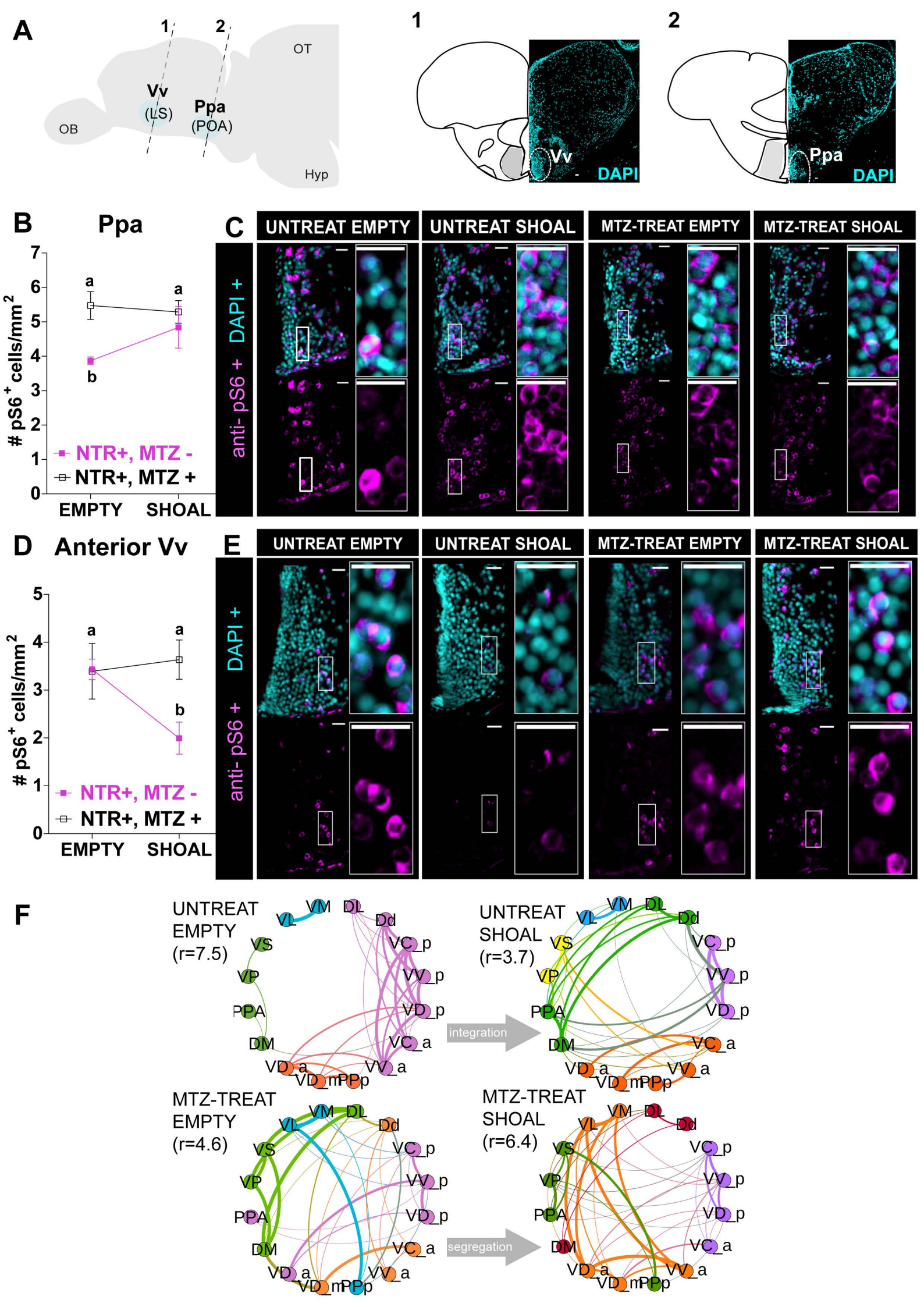
A
1
2
OT
Vv
(LS)
Ppa
(POA)
OB
Hyp
Vv
DAPI
Ppa
DAPI
B
Ppa
pS6+ cells/mm2
NTR+, MTZ -
NTR+, MTZ +
EMPTY
SHOAL
C
UNTREAT EMPTY
UNTREAT SHOAL
MTZ-TREAT EMPTY
MTZ-TREAT SHOAL
anti- pS6 +
DAPI +
D
Anterior Vv
E
F
UNTREAT EMPTY (r=7.5)
UNTREAT SHOAL (r=3.7)
MTZ-TREAT EMPTY (r=4.6)
MTZ-TREAT SHOAL (r=6.4)
integration
segregation
VM
DL
Dd
VL
VS
VP
PPA
DM
VC_p
VV_p
VD_p
VC_a
VV_a
VD_a
VD_m
PPp

Figure 6. Early-life OXT shapes social information processing. (A) Anatomical localization of the two social responsive areas: anterior part of the ventral nucleus of the ventral telencephalon (Vv_a, 1) and anterior part of the parvocellular preoptic nucleus (Ppa, 2). Brain areas identified by DAPI. (B-E) Quantification of the density (cells/mm^2) of cells expressing the neuronal marker pS6 in 4-6 days-old MTZ-treated (open squares) or untreated adult fish (full squares), after exposure to either a shoal of conspecifics or an empty tank for 10 min in the Ppa area (B) and anterior Vv area (D) and respective representative examples (C, E). Different letters indicate significant statistical differences *(p* <0.05). (F) Changes in the modular structure of functional connectivity. Modules were obtained by extracting central partition from 400 optimization of Leiden algorithm (Traag et al., 2019) on the treatment correlation matrices. Node color indicates community membership. For visualisation purposes, we only show links with correlation weight >0.1. $\boldsymbol{r}$ values indicate the ratio of total edge weight within and between modules. High (low) values of $\boldsymbol{r}$ indicate more (less) segregated modular structure.

Scale: 20 µm. Data presented as mean ± SEM.

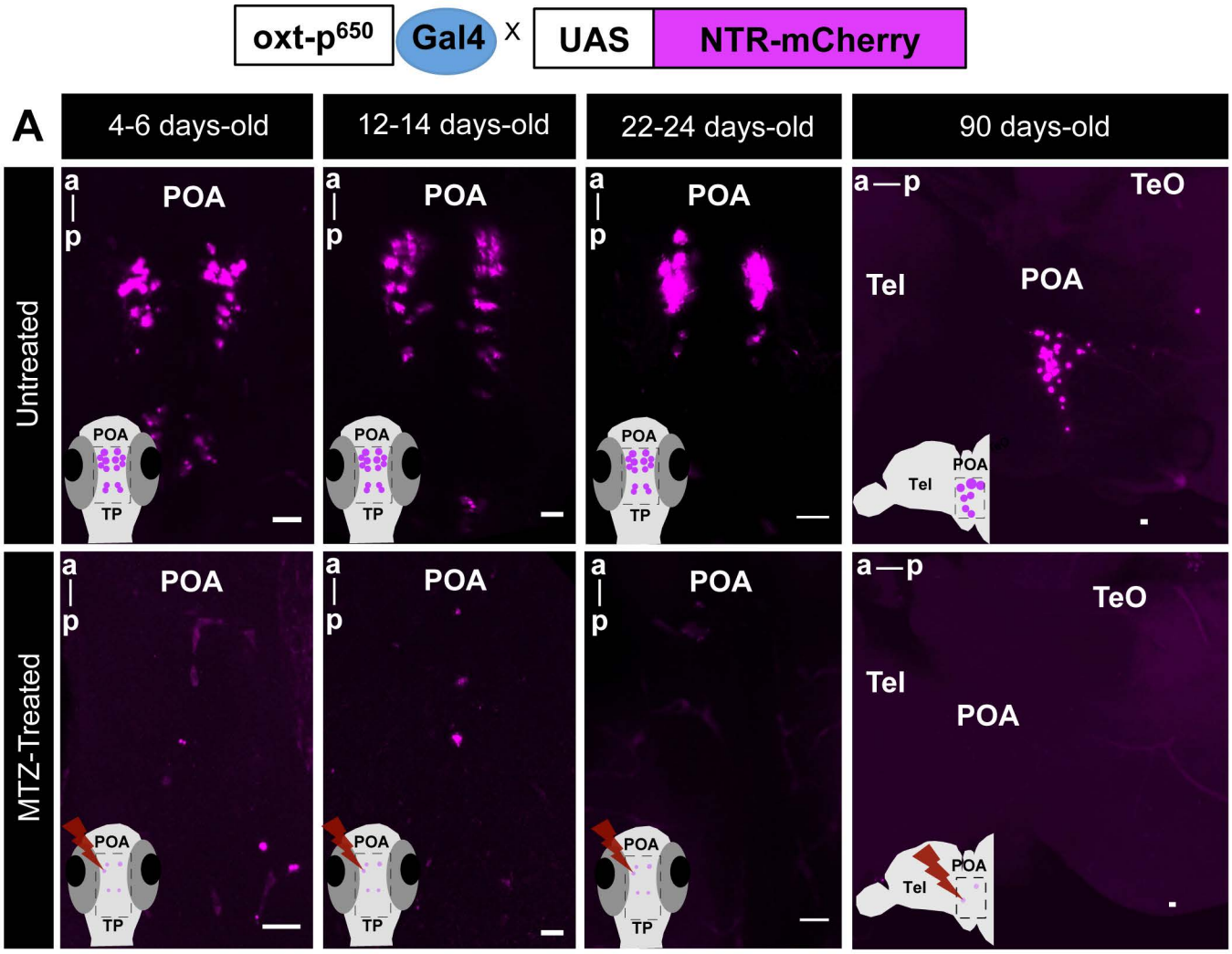
oxt-p650
Gal4
X
UAS
NTR-mCherry
A
4-6 days-old
12-14 days-old
22-24 days-old
90 days-old
Untreated
MTZ-Treated
a
p
a—p
POA
TeO
Tel
TP

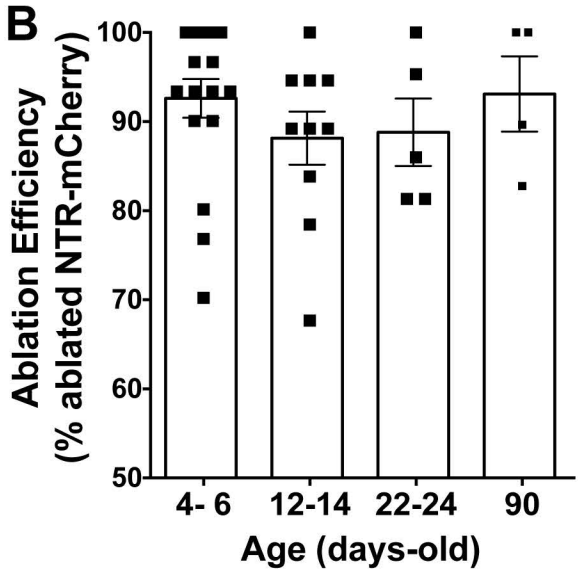
B
Ablation Efficiency
(% ablated NTR-mCherry)
100
90
80
70
60
50
4- 6
12-14
22-24
90
Age (days-old)

Figure 2-1: Spatio-temporal control of OXT-specific transgene expression.

(A) Representative example of the MTZ-treatment effect on transgene (*oxt:GAL4/UAS-NTR-mCherry*) at different treatment time-points. For 4-6, 12-14 and 22-24 days-old: whole mount larvae, maximum intensity confocal z-stack image, dorsal view, anterior to top; for 90 days-old: sagittal brain slice, maximum intensity confocal z-stack image, anterior to left. Scale: 20 μm. (B) Quantification of the effect of MTZ treatment on transgene expression at all ages tested (4-6 days-old, n=17; 12-14, n=10; 22-24 days-old, n=5; 90 days-old, n=4). Ablation efficiency was measured as percentage of ablated cells in MTZ-treated fish over mean number of NTR-mcherry cells in untreated fish. *POA*, neurosecretory preoptic area; *Tel*, Telencephalon; *TeO*, tectum optic.

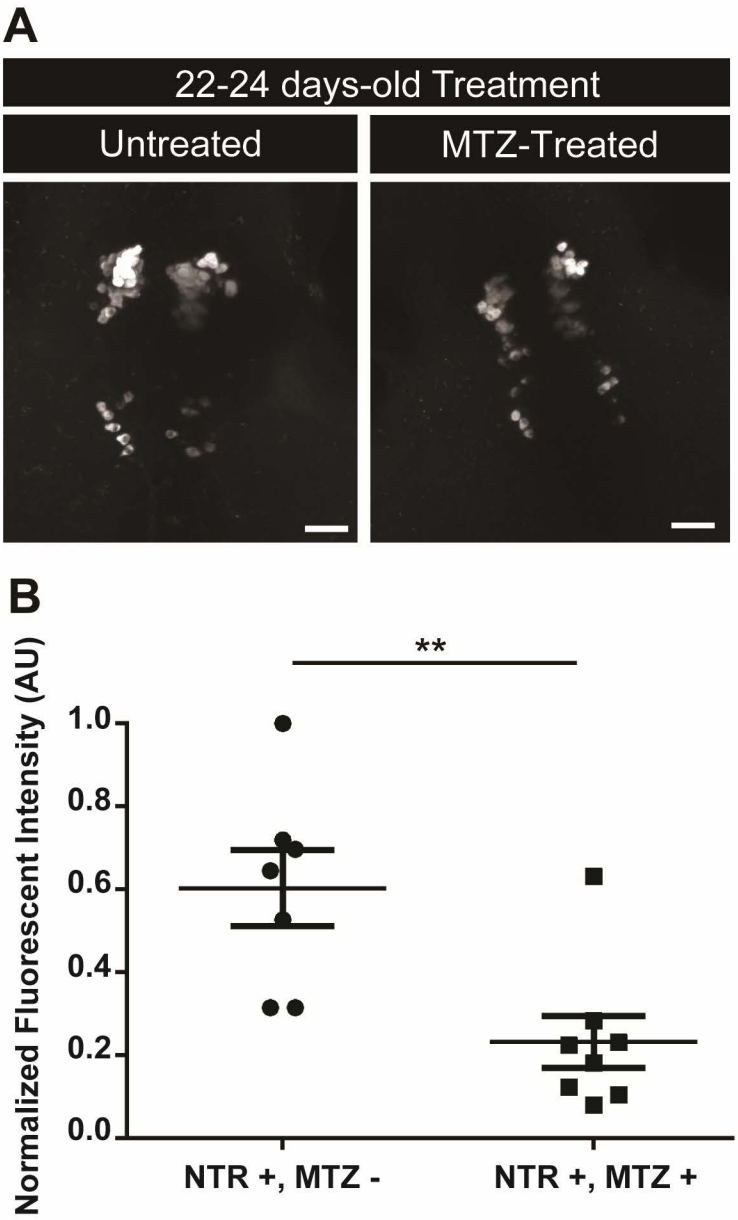
A
22-24 days-old Treatment
Untreated
MTZ-Treated
B
**
Normalized Fluorescent Intensity (AU)
1.0
0.8
0.6
0.4
0.2
0.0
NTR +, MTZ -
NTR +, MTZ +

Figure 2-2: Effects of metronidazole (MTZ)- induced ablation on endogenous OXT at 22-24 days-old treatment by in situ hybridization. (A) Representative example of the 22-24 days-old MTZ-treatment effect on endogenous OXT. Whole mount larvae, maximum intensity confocal z-stack image, dorsal view, anterior to top. Scale: 20 μm. (B) Quantification of normalized fluorescent intensity (AU) in 22-24 days-old untreated (NTR+, MTZ-) or MTZ-treated fish (NTR+, MTZ+). Data presented as mean ± SEM. **$p<0.01$

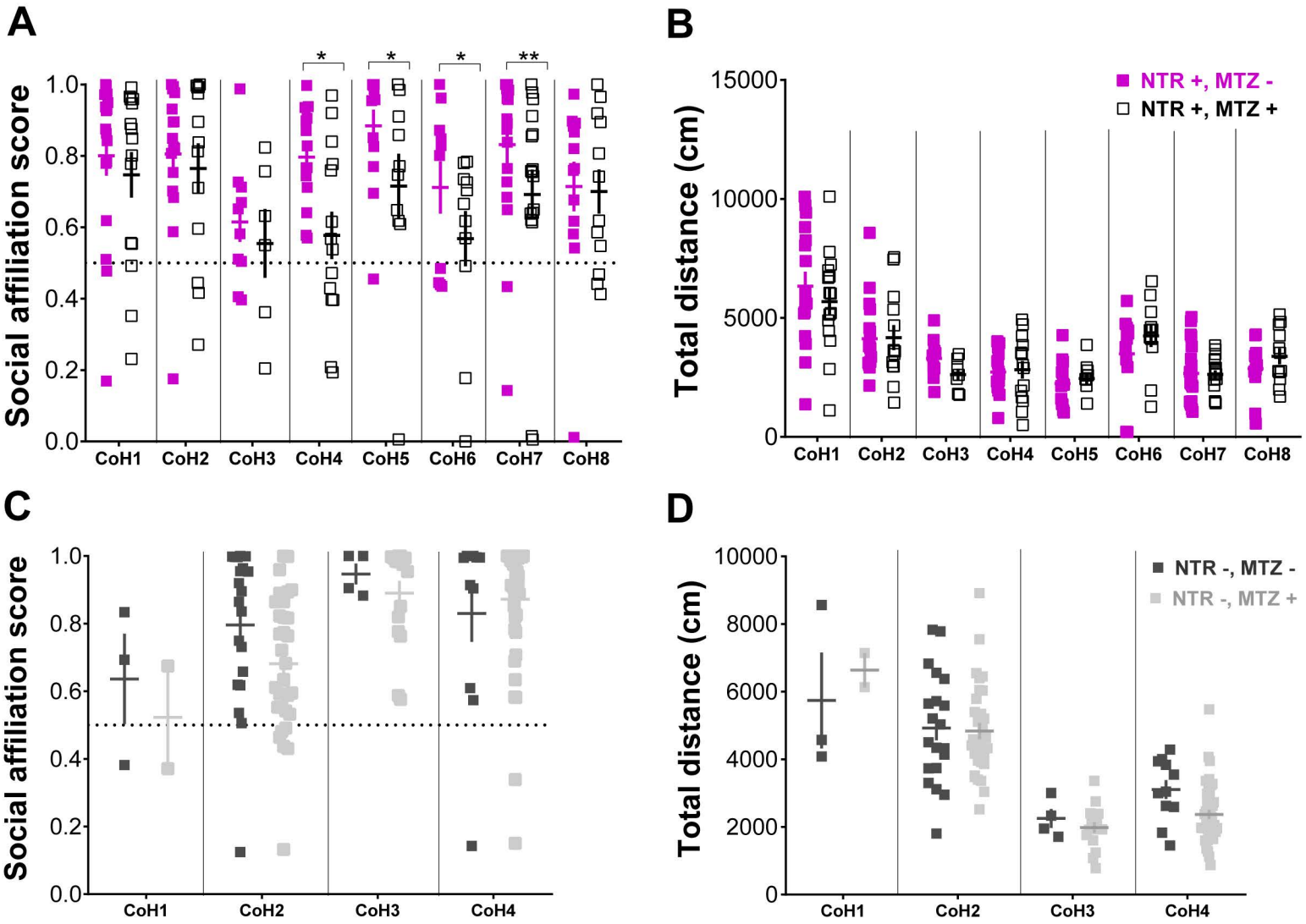
A
Social affiliation score
1.0
0.8
0.6
0.4
0.2
0.0
*
*
*
**
CoH1
CoH2
CoH3
CoH4
CoH5
CoH6
CoH7
CoH8
B
Total distance (cm)
15000
10000
5000
0
NTR +, MTZ -
NTR +, MTZ +
CoH1
CoH2
CoH3
CoH4
CoH5
CoH6
CoH7
CoH8
C
Social affiliation score
1.0
0.8
0.6
0.4
0.2
0.0
CoH1
CoH2
CoH3
CoH4
D
Total distance (cm)
10000
8000
6000
4000
2000
0
NTR -, MTZ -
NTR -, MTZ +
CoH1
CoH2
CoH3
CoH4

Figure 2-3. Organizational vs activational effects of oxytocin neurons in adult social affiliation. Effect of early (4-6 days-old) MTZ treatment on (A) adult social affiliation and (B) total distance moved of eight independent cohorts of either MTZ treated at 4-6 days-old (NTR+, MTZ+) or untreated control fish (NTR+, MTZ-); (C) adult social affiliation and (D) total distance moved of control cohorts not expressing the transgene, 4-6 days-old MTZ-treated (NTR-, MTZ+) or untreated (NTR-, MTZ-). One-tailed p-values were considered in (A) because of our *a priori* directionality hypothesis that by ablating OXT neurons, MTZ treatment of fish expressing NTR transgene would decrease social affiliation behavior. Data are presented as mean ± SEM. Full squares (purple or dark gray): untreated fish (MTZ-); open square or light gray: MTZ-treated fish (MTZ+).

Figure 2-4. Effects of 4-6 days-old MTZ treatment in adult social affiliation and total distance moved on eight independent experimental cohorts tested

Social affiliation behavior (GLM)

	d.f.1	d.f.2	F.ratio	p.value
Cohort	7	inf	2.719	0.0081**
Treatment	1	inf	9.486	0.00105**
Cohort:Treatment	7	inf	1.388	0.2053

Total Distance moved (LM)

	Df	Sum Sq	Mean Sq	F value	Pr(>F)
Cohort	7	17444	2492.03	15.2007	8.342e-16***
Treatment	1	30	30.22	0.1843	0.6681
Cohort: Treatment	7	838	119.67	0.7299	0.6468
Residuals	195	31969	163.94		

Summary of results of the GLM (Generalized Linear Model) with beta regression and LM (Linear Model) models to analyse the effects of early (4-6 days-old) MTZ-treatment on adult social affiliation and total distance moved on eight independent experimental cohorts expressing the NTR transgene. A one-tailed p-value was considered for the effect of MTZ-treatment on social affiliation behaviour because of our a priori directionality hypothesis (see Methods/Statistic section).

Figure 2-4. Effects of 4-6 days-old MTZ treatment in adult social affiliation and total distance moved on eight independent experimental cohorts tested.

Figure 2-5. Effects of 4-6 days-old MTZ-treatment in adult social affiliation and total distance moved on control fish not expressing the NTR transgene

Social affiliation behavior (GLM)

	d.f.1	d.f.2	F.ratio	p.value
Cohort	3	inf	7.249	0.0001***
Treatment	1	inf	1.241	0.2653
Cohort:Treatment	3	inf	1.271	0.2822

Total Distance moved (LM)

	Df	Sum Sq	Mean Sq	F value	Pr(>F)
Cohort	3	15614.2	5204.7	58.5513	<2e-16***
Treatment	1	183.3	183.3	2.0615	0.1536
Cohort: Treatment	3	352.1	117.4	1.3203	0.2710
Residuals	121	10755.9	88.9		

Summary of results of the GLM with beta regression and LM models to analyse the effects of early (4-6 days-old) MTZ-treatment on adult social affiliation and total distance moved on control fish not expressing the NTR transgene.

Figure 2-5. Effects of 4-6 days-old MTZ-treatment in adult social affiliation and total distance moved on control fish not expressing the NTR transgene.

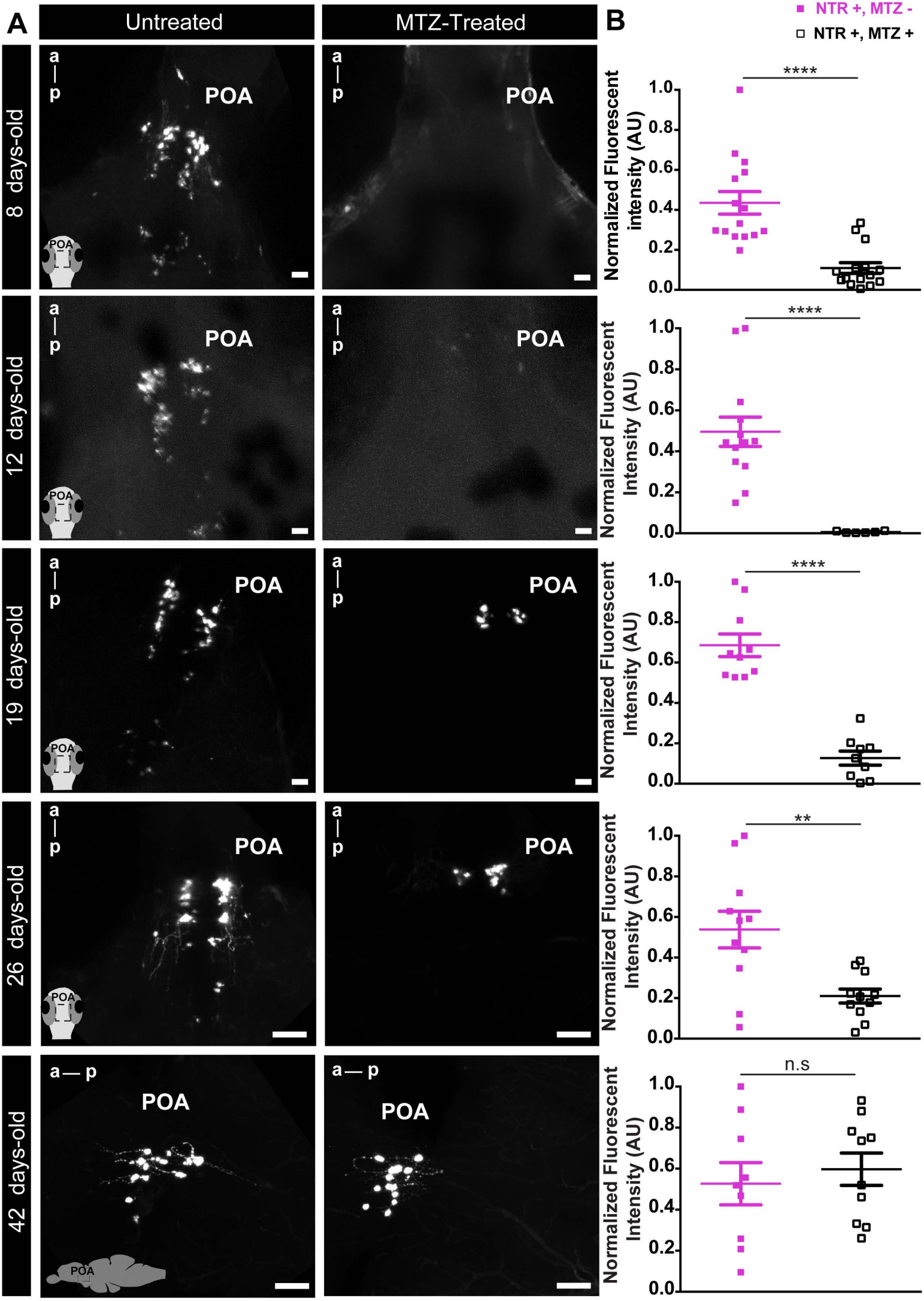
A
Untreated
MTZ-Treated
B
NTR +, MTZ -
NTR +, MTZ +
8 days-old
12 days-old
19 days-old
26 days-old
42 days-old
a
p
POA
Normalized Fluorescent intensity (AU)
Normalized Fluorescent Intensity (AU)
****
**
n.s
0.0
0.2
0.4
0.6
0.8
1.0

Figure 2-6. Time-course OXT:NTR-mCherry cell recovery after 4-6 days-old MTZ-treatment. 4-6 days-old metronidazole (MTZ)- treated *vs* untreated larvae were left to grow and sampled at different time-points throughout development: 8, 12, 19, 26, and 42 days-old. A) Representative whole mount larvae, maximum intensity confocal z-stack image, dorsal view, anterior to top (8, 12, 19 and 26 days-old) and sagittal brain slice, confocal z-stack image, anterior to left (42 days-old). B) Quantification of the Normalized fluorescent intensity (AU) in untreated (full squares) versus MTZ-treated fish (open squares) at the different time points sampled.

Scale: 20 μm (8-12-19-days-old) and 50 μm (26 and 42 days-old). Data are presented as mean ± SEM. Full squares: untreated fish (NTR+,MTZ-); open square: MTZ-treated fish (NTR+,MTZ+). **$p<0.01$,**** $p<0.0001$

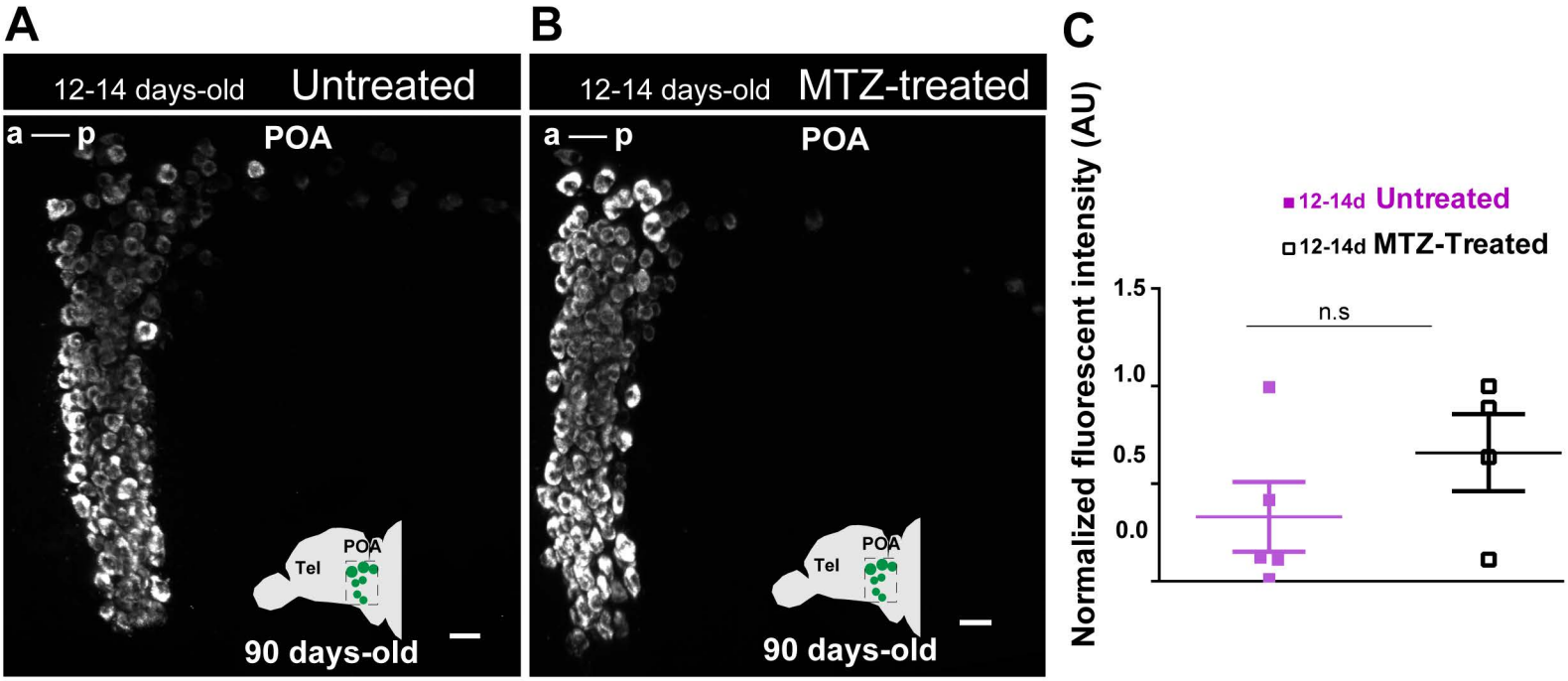
A
12-14 days-old
Untreated
a — p
POA
Tel
POA
90 days-old
B
12-14 days-old
MTZ-treated
a — p
POA
Tel
POA
90 days-old
C
Normalized fluorescent intensity (AU)
12-14d Untreated
12-14d MTZ-Treated
1.5
1.0
0.5
0.0
n.s

Figure 2-7. Endogenous OXT mRNA recovery in adulthood after 12-14 days-old MTZ-treatment. (A) Representative example of the endogenous OXT mRNA in untreated adult fish. (B) Representative example of the endogenous OXT mRNA in adult fish treated with MTZ at 12-14 days-old. Images in (A,B) are maximum intensity confocal z-stacks, sagittal slices, anterior to left. Scale: 20 μm. (C) Quantification of normalized fluorescent intensity (AU) in untreated (full squares) and 12-14 days-old MTZ-treated adult fish (empty squares). Data presented as mean ± SEM. Full squares: untreated fish (NTR+,MTZ-); open square: MTZ-treated fish (NTR+,MTZ+).

Figure 3-1. Effect of 4-6 days-old MTZ-treatment in TH cell clusters of larvae zebrafish brain. Three independent brain areas were analyzed. Linear model with post-hoc tests comparing the treatment (early MTZ-treated vs. untreated) were performed.

BA	Treat1	Treat2	estim	SE	z.ratio	*p*.value
Subpallium	Untreated	MTZ-Treated	-2.889	2.622	-1.102	0.278
PrT	Untreated	MTZ-Treated	-8.278	2.994	-2.764	0.009 **
TP Large cells	Untreated	MTZ-Treated	-1.722	0.566	-3.042	0.0045**

BA, Brain area; *Treat*, Treatment; *estim*, estimate; *PrT,* Pretectum; *TP*, Posterior Tuberculum.

Figure 3-1. Effect of 4-6 days-old MTZ-treatment in TH cell clusters of larvae zebrafish brain. Three independent brain areas were analyzed. Linear model with post-hoc tests comparing the treatment (early MTZ-treated vs. untreated) were performed.

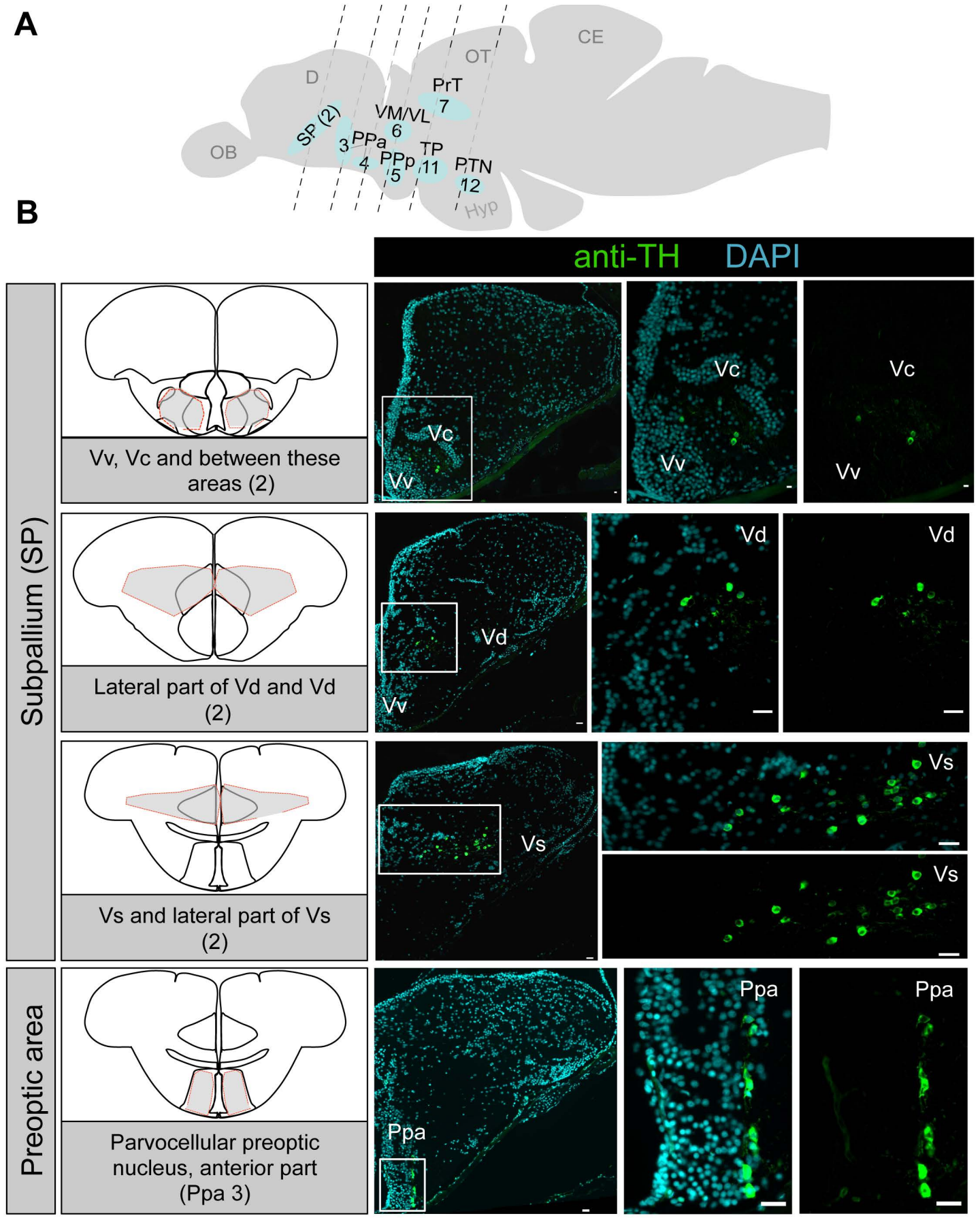
A
CE
OT
D
PrT
7
VM/VL
6
SP (2)
3
PPa
4
PPp
5
TP
11
PTN
12
OB
Hyp
B
anti-TH
DAPI
Subpallium (SP)
Vv, Vc and between these areas (2)
Vc
Vv
Lateral part of Vd and Vd (2)
Vd
Vs and lateral part of Vs (2)
Vs
Preoptic area
Parvocellular preoptic nucleus, anterior part (Ppa 3)
Ppa

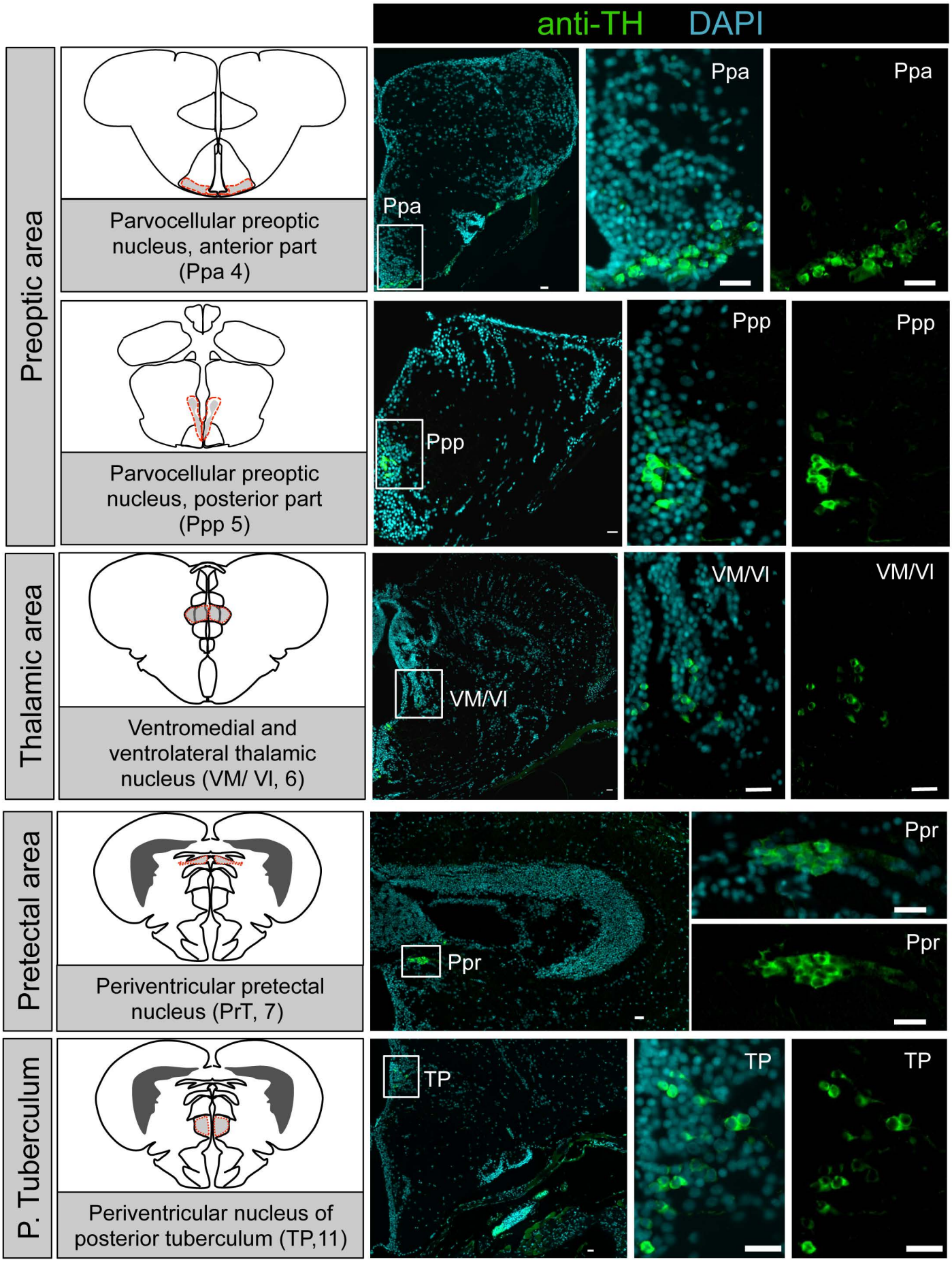
anti-TH DAPI
Preoptic area
Parvocellular preoptic nucleus, anterior part (Ppa 4)
Ppa
Ppa
Ppa
Parvocellular preoptic nucleus, posterior part (Ppp 5)
Ppp
Ppp
Ppp
Thalamic area
Ventromedial and ventrolateral thalamic nucleus (VM/ Vl, 6)
VM/Vl
VM/Vl
VM/Vl
Pretectal area
Periventricular pretectal nucleus (PrT, 7)
Ppr
Ppr
Ppr
P. Tuberculum
Periventricular nucleus of posterior tuberculum (TP,11)
TP
TP
TP

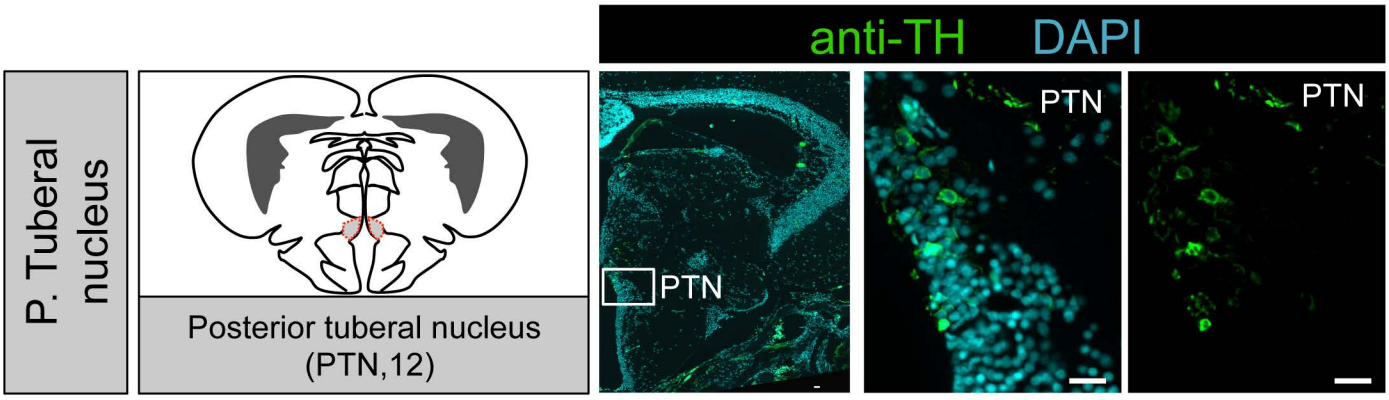
anti-TH
DAPI
P. Tuberal nucleus
Posterior tuberal nucleus
(PTN,12)
PTN
PTN
PTN

Figure 4-1 - Early life OXT ablation affects the dopaminergic system. (A) Schematic representation of an adult zebrafish sagittal view representing the coronal sections of all dopaminergic areas sampled in the adult brain (dopaminergic cluster nomenclature according to(Panula et al., 2010)). (B) Schematic representation of zebrafish brain coronal sections highlighting the different dopaminergic clusters (adapted from (Wullimann et al., 1996)) and representative example showing anatomical localization of the dopaminergic groups in an untreated adult zebrafish. Landmarks of the areas identified by DAPI (cyan) and dopaminergic groups by TH (Tyrosine Hydroxylase) immunostaining (green). Scale bars are 20μm.

Figure 4-2. Effect of 4-6 days-old MTZ-treatment in TH cell clusters of adult zebrafish brain. Eight independent brain areas were analyzed. GLMM with a Poisson regression and planned comparisons (early MTZ-Treated vs. Untreated) was performed. *p*-values from planned comparisons were corrected with false discovery rate (FDR) adjustment method.

BA	Treat1	Treat2	estim	SE	z.ratio	*p*.value. indep. GLMM	*p*.value. indep. GLMM. fdr correction
Subpallium (G2)	Untreated	MTZ-Treated	-0.031	0.0562	-0.552	0.5813	0.6643
PPa (G3)	Untreated	MTZ-Treated	0.185	0.175	1.058	0.2901	0.3868
PPa (G4)	Untreated	MTZ-Treated	0.0611	0.0533	1.147	0.2513	0.3868
PPp (G5)	Untreated	MTZ-Treated	0.12	0.0747	1.603	0.1090	0.218
Vm + Vl (G6)	Untreated	MTZ-Treated	0.0143	0.0755	0.189	0.8502	0.8502
PrT (G7)	Untreated	MTZ-Treated	0.201	0.0598	3.364	0.0008	0.0048**
TP (G11)	Untreated	MTZ-Treated	0.188	0.0724	2.597	0.0094	0.0251*
PTN (G12)	Untreated	MTZ-Treated	0.19	0.0586	3.239	0.0012	0.0048**

BA, Brain area; *Treat*, Treatment; *estim*, estimate; *GLMM*, Generalized Linear Mixed Models; *FDR*, false discovery rate, *PPa*, anterior part of the parvocellular preoptic nucleus; *PPp*, posterior part of the Parvocellular preoptic nucleus; *Vm*, ventromedial thalamic nucleus; *Vl*, ventrolateral thalamic nucleus; *PrT*, Pretectum nucleus; *TP*, Posterior tuberculum nucleus; *PTN*, Posterior Tuberal nucleus.

Figure 4-2. Effect of 4-6 days-old MTZ-treatment in TH cell clusters of adult zebrafish brain. Eight independent brain areas were analyzed. GLMM with a Poisson regression and planned comparisons (early MTZ-Treated vs. Untreated) was performed. *p*-values from planned comparisons were corrected with false discovery rate (FDR) adjustment method.

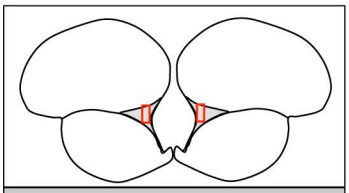

Dorsal nucleus of the ventral telencephalic area (anterior) Vd_a

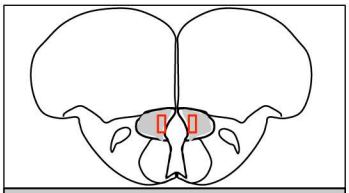

Dorsal nucleus of the ventral telencephalic area (medial) Vd_m

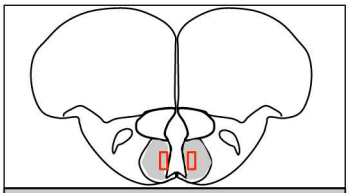

Ventral nucleus of the ventral telencephalic area (anterior) Vv_a

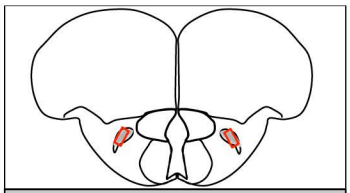

Central nucleus of the ventral telencephalic area (anterior) Vc_a

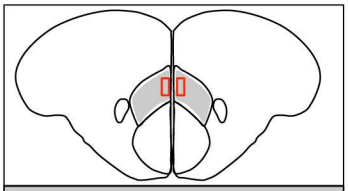

Dorsal nucleus of the ventral telencephalic area (posterior) Vd_p

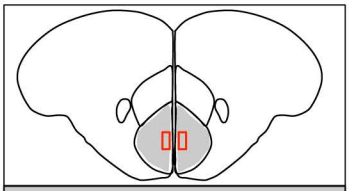

Ventral nucleus of the ventral telencephalic area (posterior) Vv_p

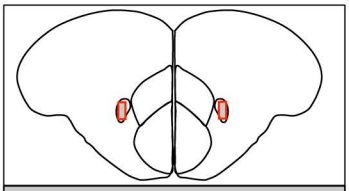

Central nucleus of the ventral telencephalic area (posterior) Vc_p

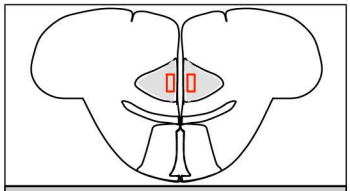

Supracommissural nucleus of the ventral telencephalic area, Vs

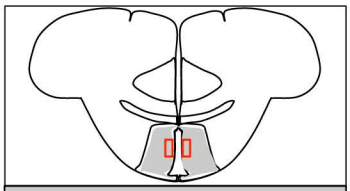

Parvocellular preoptic nucleus, anterior part Ppa

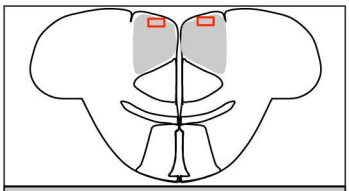

Medial part of the Dorsal telencephalic area, Dm

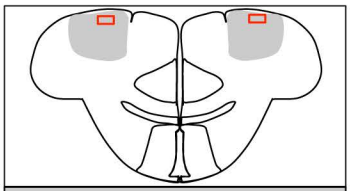

Dorsal part of the Dorsal telencephalic area, Dd

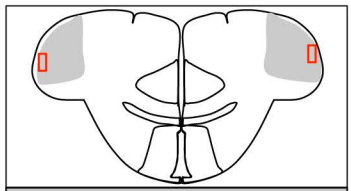

Lateral part of the Dorsal telencephalic area, Dl

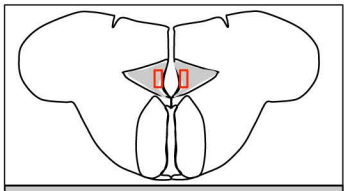

Postcommissural nucleus of the ventral telencephalic area, Vp

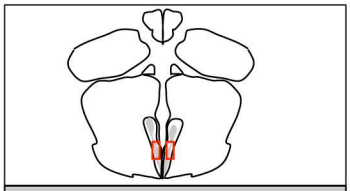

Parvocellular preoptic nucleus, posterior part, Ppp

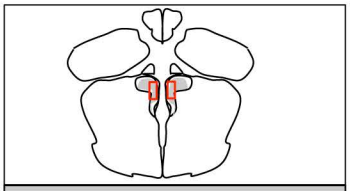

Ventromedial thalamic nucleus Vm

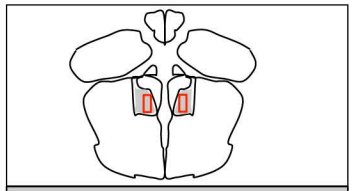

Ventrolateral thalamic nucleus Vl

Figure 6-1. Schematic representation of brain areas that were analyzed for neuronal activation in response to social stimulus. pS6 immunostaining served as a readout of neuronal activation following MTZ treatment at 4-6 days-old or untreated adult fish to either a shoal of conspecifics or an empty tank. Included brain areas are part of the social decision-making network, subdivided into more anterior or posterior parts. Schematics are adapted from zebrafish atlas (Wullimann et al., 1996).

Figure 6-2. Effect of 4-6 days-old MTZ-treatment on adult neuronal activation. Neuronal activation measured by pS6 immunostaining. Sixteen (16) independent brain areas were analyzed. GLMM with a Poisson regression and planned comparisons were performed. *p*-values of the planned comparisons were corrected with false discovery rate (FDR) adjustment method (significant values in red).

BA1	Stim1	Treat1	BA2	Stim2	Treat2	estim	SE	z.ratio	*p*.value. indep. GLMM	*p*.value. indep. GLMM. fdr correction
Dd	EMPTY	CTR	Dd	SHOAL	CTR	-0.2076	0.125	-1.655	0.0978	0.4084
Dd	EMPTY	ABLAT	Dd	EMPTY	CTR	-0.2057	0.147	-1.399	0.1618	0.523687
Dd	SHOAL	ABLAT	Dd	SHOAL	CTR	-0.0078	0.118	-0.066	0.9477	0.9683302
Dd	EMPTY	ABLAT	Dd	SHOAL	ABLAT	-0.0096	0.138	-0.069	0.9448	0.9683302
DL	EMPTY	CTR	DL	SHOAL	CTR	-0.096	0.0948	-1.013	0.311	0.7052
DL	EMPTY	ABLAT	DL	EMPTY	CTR	-0.1449	0.1067	-1.359	0.1743	0.523687
DL	SHOAL	ABLAT	DL	SHOAL	CTR	-0.1496	0.0831	-1.8	0.0718	0.4084
DL	EMPTY	ABLAT	DL	SHOAL	ABLAT	-0.1007	0.0964	-1.044	0.2964	0.7025778
DM	EMPTY	CTR	DM	SHOAL	CTR	-0.0206	0.118	-0.174	0.8617	0.9347254
DM	EMPTY	ABLAT	DM	EMPTY	CTR	-0.0238	0.135	-0.177	0.8598	0.9347254
DM	SHOAL	ABLAT	DM	SHOAL	CTR	-0.1401	0.105	-1.332	0.1827	0.523687
DM	EMPTY	ABLAT	DM	SHOAL	ABLAT	-0.1369	0.124	-1.107	0.2683	0.6604308
PPA	**EMPTY**	**CTR**	**PPA**	**SHOAL**	**CTR**	**-0.2858**	**0.0899**	**-3.18**	**0.0015**	**0.024**
PPA	**EMPTY**	**ABLAT**	**PPA**	**EMPTY**	**CTR**	**0.3415**	**0.1018**	**3.356**	**0.0008**	**0.024**
PPA	SHOAL	ABLAT	PPA	SHOAL	CTR	0.017	0.0793	0.215	0.83	0.9347254
PPA	EMPTY	ABLAT	PPA	SHOAL	ABLAT	0.0387	0.0926	0.418	0.6761	0.8830694
PPp	EMPTY	CTR	PPp	SHOAL	CTR	-0.2579	0.116	-2.229	0.0258	0.2638222
PPp	EMPTY	ABLAT	PPp	EMPTY	CTR	-0.1959	0.129	-1.521	0.1284	0.4833882
PPp	SHOAL	ABLAT	PPp	SHOAL	CTR	-0.0306	0.103	-0.297	0.7663	0.9082074
PPp	EMPTY	ABLAT	PPp	SHOAL	ABLAT	-0.0926	0.117	-0.789	0.4302	0.795241
VC_a	EMPTY	CTR	VC_a	SHOAL	CTR	0.0668	0.141	0.474	0.6358	0.8830694
VC_a	EMPTY	ABLAT	VC_a	EMPTY	CTR	-0.3189	0.153	-2.085	0.0371	0.2638222
VC_a	SHOAL	ABLAT	VC_a	SHOAL	CTR	-0.2749	0.132	-2.085	0.0371	0.2638222
VC_a	EMPTY	ABLAT	VC_a	SHOAL	ABLAT	0.1107	0.144	0.767	0.4433	0.795241
VC_p	EMPTY	CTR	VC_p	SHOAL	CTR	-0.0203	0.133	-0.153	0.8786	0.9371733
VC_p	EMPTY	ABLAT	VC_p	EMPTY	CTR	-0.1035	0.146	-0.708	0.4789	0.795241
VC_p	SHOAL	ABLAT	VC_p	SHOAL	CTR	-0.0401	0.116	-0.347	0.7285	0.9082074
VC_p	EMPTY	ABLAT	VC_p	SHOAL	ABLAT	0.0431	0.131	0.33	0.7417	0.9082074
VD_a	EMPTY	CTR	VD_a	SHOAL	CTR	-0.2073	0.161	-1.287	0.1981	0.5282667
VD_a	EMPTY	ABLAT	VD_a	EMPTY	CTR	-0.1121	0.17	-0.659	0.5102	0.81632
VD_a	SHOAL	ABLAT	VD_a	SHOAL	CTR	0.0089	0.152	0.059	0.9532	0.9683302
VD_a	EMPTY	ABLAT	VD_a	SHOAL	ABLAT	-0.0862	0.162	-0.533	0.5942	0.8830694
VD_m	EMPTY	CTR	VD_m	SHOAL	CTR	0.0482	0.115	0.419	0.6749	0.8830694
VD_m	EMPTY	ABLAT	VD_m	EMPTY	CTR	-0.2684	0.125	-2.147	0.0318	0.2638222
VD_m	SHOAL	ABLAT	VD_m	SHOAL	CTR	-0.0759	0.109	-0.699	0.4846	0.795241
VD_m	EMPTY	ABLAT	VD_m	SHOAL	ABLAT	0.2407	0.119	2.016	0.0438	0.28032
VD_p	EMPTY	CTR	VD_p	SHOAL	CTR	0.112	0.114	0.985	0.3247	0.7052
VD_p	EMPTY	ABLAT	VD_p	EMPTY	CTR	-0.169	0.125	-1.355	0.1754	0.523687
VD_p	SHOAL	ABLAT	VD_p	SHOAL	CTR	-0.173	0.104	-1.661	0.0968	0.4084
VD_p	EMPTY	ABLAT	VD_p	SHOAL	ABLAT	0.108	0.116	0.932	0.3513	0.7052
VL	EMPTY	CTR	VL	SHOAL	CTR	0.00959	0.328	0.029	0.9767	0.9767
VL	EMPTY	ABLAT	VL	EMPTY	CTR	0.06954	0.365	0.19	0.8491	0.9347254

VL	SHOAL	ABLAT	VL	SHOAL	CTR	0.14089	0.309	0.455	0.6489	0.8830694
VL	EMPTY	ABLAT	VL	SHOAL	ABLAT	0.08094	0.349	0.232	0.8165	0.9347254
VM	EMPTY	CTR	VM	SHOAL	CTR	-0.3257	0.265	-1.231	0.2184	0.559104
VM	EMPTY	ABLAT	VM	EMPTY	CTR	0.1426	0.299	0.476	0.6339	0.8830694
VM	SHOAL	ABLAT	VM	SHOAL	CTR	0.3621	0.248	1.461	0.144	0.512
VM	EMPTY	ABLAT	VM	SHOAL	ABLAT	-0.1062	0.285	-0.373	0.7089	0.907392
VP	EMPTY	CTR	VP	SHOAL	CTR	-0.2041	0.123	-1.663	0.0963	0.4084
VP	EMPTY	ABLAT	VP	EMPTY	CTR	-0.1158	0.145	-0.8	0.4234	0.795241
VP	SHOAL	ABLAT	VP	SHOAL	CTR	0.1484	0.113	1.316	0.1882	0.523687
VP	EMPTY	ABLAT	VP	SHOAL	ABLAT	0.06	0.135	0.446	0.6559	0.8830694
VS	EMPTY	CTR	VS	SHOAL	CTR	-0.3116	0.117	-2.664	0.0077	0.09856
VS	EMPTY	ABLAT	VS	EMPTY	CTR	-0.1251	0.133	-0.938	0.3483	0.7052
VS	SHOAL	ABLAT	VS	SHOAL	CTR	0.0968	0.104	0.93	0.3526	0.7052
VS	EMPTY	ABLAT	VS	SHOAL	ABLAT	-0.0897	0.122	-0.734	0.4628	0.795241
VV_a	**EMPTY**	**CTR**	**VV_a**	**SHOAL**	**CTR**	**0.6076**	**0.19**	**3.193**	**0.0014**	**0.024**
VV_a	EMPTY	ABLAT	VV_a	EMPTY	CTR	0.0626	0.205	0.305	0.7606	0.9082074
VV_a	**SHOAL**	**ABLAT**	**VV_a**	**SHOAL**	**CTR**	**-0.6333**	**0.181**	**-3.504**	**0.0005**	**0.024**
VV_a	EMPTY	ABLAT	VV_a	SHOAL	ABLAT	-0.0883	0.197	-0.449	0.6537	0.8830694
VV_p	EMPTY	CTR	VV_p	SHOAL	CTR	0.0579	0.114	0.509	0.611	0.8830694
VV_p	EMPTY	ABLAT	VV_p	EMPTY	CTR	-0.2034	0.124	-1.635	0.1021	0.4084
VV_p	SHOAL	ABLAT	VV_p	SHOAL	CTR	-0.1748	0.104	-1.687	0.0915	0.4084
VV_p	EMPTY	ABLAT	VV_p	SHOAL	ABLAT	0.0865	0.115	0.751	0.4529	0.795241

BA1, Brain area 1; *BA2*, Brain area 2; *Stim*, stimulus; *Treat*, Treatment; *estim*, estimate; *indep*., independent, *GLMM*, Generalized Linear Mixed Models; *FDR*, false discovery rate, *CTR*, untreated fish; *ABLT*, early MTZ-treated fish; *Vv_a*, anterior part of the ventral nucleus of the ventral telencephalic area (V); *Vv_p*, posterior part of the ventral nucleus of the ventral telencephalic area (V); *Vd_a*, anterior part of the dorsal nucleus of V; *Vd_m*, medial part of the dorsal nucleus of V; *Vd_p*, posterior part of the dorsal nucleus of V; *Vc_a*, anterior part of the central nucleus of V; *Vc_p*, posterior part of the central nucleus of V; *Dm*, medial zone of the dorsal telencephalic area (D); *Dl*, lateral zone of the dorsal telencephalic area (D); *Dd*, dorsal zone of the dorsal telencephalic area (D); *Vs*, supracommissural nucleus of V; *Vp*, postcommissural nucleus of V; *Ppa*, anterior part of the parvocellular preoptic nucleus; *Ppp*, posterior part of the parvocellular preoptic nucleus; *VM*, ventromedial thalamic nucleus; *VL*, ventrolateral thalamic nucleus.

Figure 6-2. Effect of 4-6 days-old MTZ-treatment on adult neuronal activation. Neuronal activation measured by pS6 immunostaining. Sixteen (16) independent brain areas were analyzed. GLMM with a Poisson regression and planned comparisons were performed. p-values of the planned comparisons were corrected with false discovery rate (*FDR*) adjustment method (significant values in red).

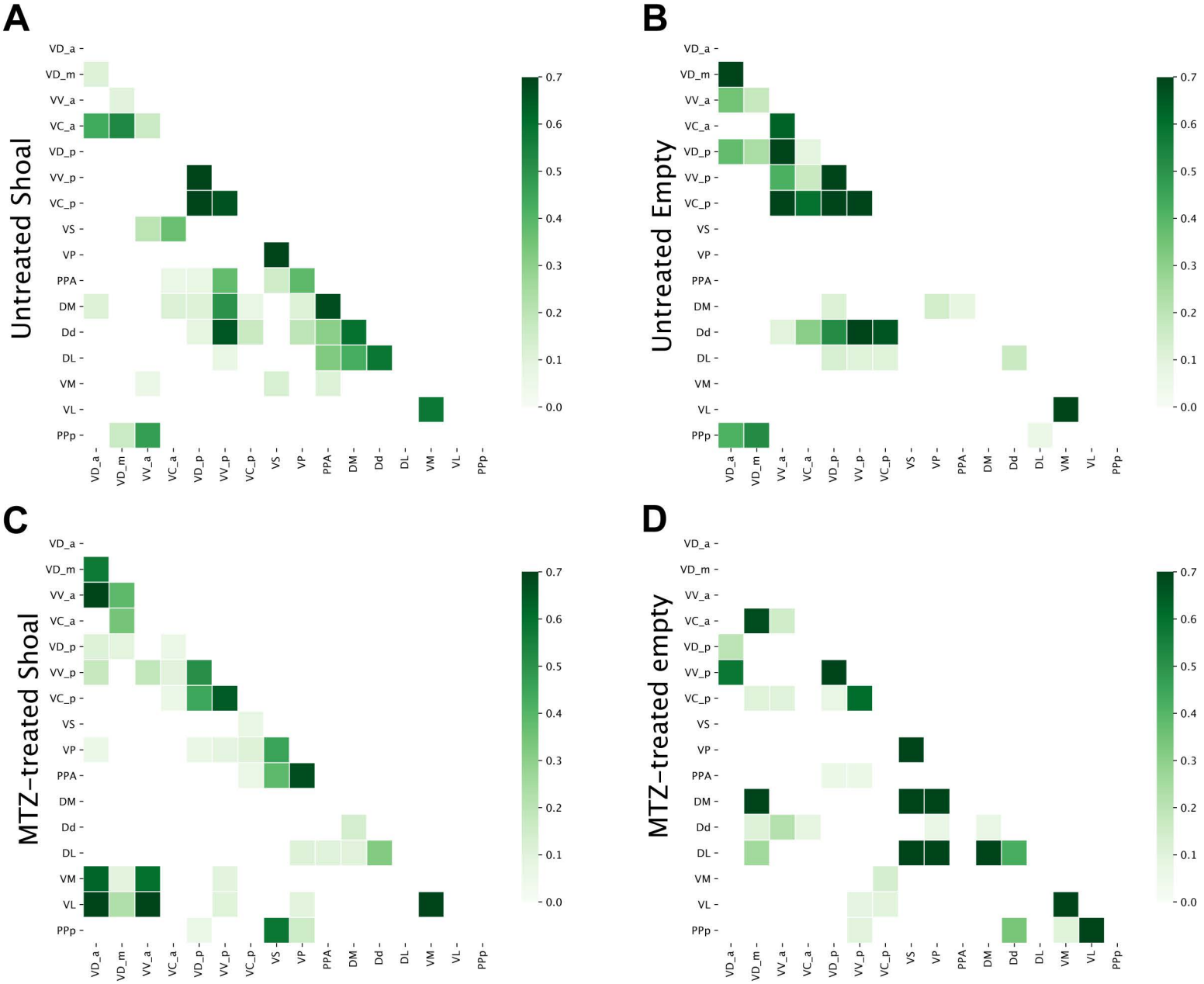
A
Untreated Shoal
B
Untreated Empty
C
MTZ-treated Shoal
D
MTZ-treated empty
VD_a
VD_m
VV_a
VC_a
VD_p
VV_p
VC_p
VS
VP
PPA
DM
Dd
DL
VM
VL
PPp
0.7
0.6
0.5
0.4
0.3
0.2
0.1
0.0

Figure 6-3. Correlation matrices of functional connectivity for the four treatments reveal early-life OXT shapes social information processing. Regional correlation values are computed joining data from both hemispheres. Resampled correlations were kept if significant ($p<0.05$). For visualisation purposes, we show only entries of significant correlations higher than 0.05.

Figure 6-4. Rank of node strength centralities of adult treated Vs untreated zebrafish, exposed to a conspecific shoal or to empty compartments.

Rank	AE	AS	CE	CS
1	DM	VD_a	VD_p	VV_p
2	DL	VL	VC_p	DM
3	VS	VV_a	VV_a	Dd
4	VP	VM	VV_p	PPA
5	VV_p	VV_p	Dd	VD_p
6	VD_m	VP	VD_a	VC_p
7	VL	VD_m	VC_a	VC_a
8	Dd	VS	VD_m	VS
9	PPp	VC_p	PPp	VP
10	VD_p	VD_p	VL	DL
11	VM	PPA	VM	VV_a
12	VC_p	PPp	DL	VD_m
13	VC_a	DL	DM	VM
14	VD_a	VC_a	VP	VD_a
15	VV_a	Dd	PPA	PPp
16	PPA	DM	VS	VL

AE, early-MTZ treated fish exposed to empty compartment; *AS*, early MTZ-treated fish exposed to shoal; CE, untreated fish exposed to empty compartment; CS, untreated fish exposed to shoal; *Vv_a*, anterior part of the ventral nucleus of the ventral telencephalic area (V); *Vv_p*, posterior part of the ventral nucleus of the ventral telencephalic area (V); *Vd_a*, anterior part of the dorsal nucleus of V; *Vd_m*, medial part of the dorsal nucleus of V; *Vd_p*, posterior part of the dorsal nucleus of V; *Vc_a*, anterior part of the central nucleus of V; *Vc_p*, posterior part of the central nucleus of V; *Dm*, medial zone of the dorsal telencephalic area (D); *Dl*, lateral zone of the dorsal telencephalic area (D); *Dd*, dorsal zone of the dorsal telencephalic area (D); *Vs*, supracommissural nucleus of V; *Vp*, postcommissural nucleus of V; *Ppa*, anterior part of the parvocellular preoptic nucleus; *Ppp*, posterior part of the parvocellular preoptic nucleus; *VM*, ventromedial thalamic nucleus; *VL*, ventrolateral thalamic nucleus;

Figure 6-4. Rank of node strength centralities of adult treated vs untreated zebrafish, exposed to a conspecific shoal or to empty compartments.